WAVE ATTENUATION OF NATURAL AND NATURE-BASED FEATURES: COMPARING EXPLICIT AND IMPLICIT FORMULATIONS

by

Tyler Miesse

A Thesis
Submitted to the
Graduate Faculty
of
George Mason University
in Partial Fulfillment of
The Requirements for the Degree
of
Master of Science
Civil, Environmental, and Infrastructure Engineering

Committee:

_____ Dr. Celso Ferreira, Thesis Director

_____ Dr. Lucas Henneman, Committee Member

_____ Dr. Viviana Maggioni, Committee Member

_____ Dr. Sam Salem, Department Chair

_____ Dr. Kenneth S. Ball, Dean, Volgenau School of Engineering

Date: _____ Spring Semester 2021
George Mason University
Fairfax, VA

Wave Attenuation of Natural and Nature-Based Features: Comparing Explicit and Implicit Formulations

A Thesis submitted in partial fulfillment of the requirements for the degree of Master of Science at George Mason University

by

Tyler Miesse
Bachelor of Science
George Mason University, 2019

Director: Celso Ferreira, Associate Professor
Department of Civil, Environmental, and Infrastructure Engineering

Spring Semester 2021
George Mason University
Fairfax, VA

DEDICATION

This is dedicated to my family and my friends in the Flood Hazards Research Lab. My parents and my sister have provided me with invaluable support for my research, and my dog, Buxton, who likes to represent the Flood Hazards Research Lab.

ACKNOWLEDGEMENTS

The author wishes to thank the Texas Advanced Computing Center (TACC) of The University of Texas at Austin for providing the High-Performance Computing resources necessary. In this work, we utilized the Extreme Science and Engineering Discovery Environment (XSEDE) STAMPEDE2 resources through allocation id TG-BCS130009, which is supported by National Science Foundation [grant number ACI- 1548562] (Towns et al., 2014). Data was collected as part of the During Nearshore Event Experiment (DUNEX), which was facilitated by the U.S. Coastal Research Program (USCRP). We thank USCRP for their support through funding for logistics and coordination.

TABLE OF CONTENTS

LIST OF TABLES

LIST OF FIGURES

LIST OF EQUATIONS

ABSTRACT

WAVE ATTENUATION OF NATURAL AND NATURE-BASED FEATURES: COMPARING EXPLICIT AND IMPLICIT FORMULATIONS

Tyler Miesse, M.S.

George Mason University, 2021

Thesis Director: Dr. Celso Ferreira

Coastal communities are highly exposed to waves and storm surge during extreme events. One option for protecting coastal communities that has gained popularity during the last decade is the use of natural and nature-based features (NNBF). Data documenting the flood protection capacity of these systems, especially related to the attenuation of wave energy during extreme events, is a key limiting factor to the understanding of NNBF functions as each site has unique characteristics based on vegetation, geology, and historical context. To address the need for more information on the benefits of NNBFs for coastal protection, recent advances in numerical models have incorporated the interaction of the vegetation with hydrodynamics and waves. The current state of the art models represents the vegetation in one of two ways: (1) “explicit” interactions between waves and vegetation through “site-specific” data on the stem height, stem diameter, and the plant density, and (2) “implicit” representation through equivalent bottom roughness length derived from landcover datasets at the National and Regional scale. While the explicit formulation

provides higher fidelity in terms of physical processes representation, it requires local information that is typically unavailable for most locations. To evaluate the possible options of wave attenuation this study focuses on two different marshes in the Chesapeake Bay to investigate: 1) the fidelity of the implicit and explicit representation of wave attenuation by vegetation, and 2) the accuracy of numerical models at varying geographical domains and resolutions in calculating the wave attenuation by vegetation. This study compared two different numerical models that can be applied at different geographical scales: a local scale model which is a site-specific domain, and a regional model that has a domain of the United States east coast. Ultimately, this study found that the explicit approach and finer resolution models improved the accuracy of the wave attenuation calculation. When looking at a regional perspective, the implicit approach would provide a 30% underestimation of the wave attenuation at the edge of the marsh, but it will show full attenuation of the wave energy within marsh, when marsh lengths exceed 400m, which would still provide guidance on possible protection strategies.

CHAPTER 1: INTRODUCTION

Background

Coastal communities are highly exposed to waves and storm surge during extreme events. For instance, Hurricane Dorian devastated the southern and mid-Atlantic coast of the United States in 2019, causing up to USD 3 billion in damages and up to 70 deaths (Lynn Jenner, 2019). One option for protecting coastal communities that has gained popularity during the last decade is the use of natural and nature-based features (NNBF) (Sutton-Grier et al, 2015). These green infrastructure options are being considered as coastal defense alternatives since they provide shoreline protection by damping incoming waves and depositing sediment in vegetated regions (Van Coppenolle et al., 2018). NNBFs, such as coastal ecosystems, play a crucial role in: i) reducing the coastal risk of flooding, ii) dissipating waves, iii) providing sheltered environments where (fine) sediments can settle (Feagin et al., 2009), iv) providing a habitat for numerous species , and v) lastly for carbon sequestration (Arkema et al., 2013; Crooks et al., 2018; Hladik et al., 2013). The understanding of the specific risk reduction functions of NNBF approaches is still limited (Cavaleri et al. 2018; Elko et al., 2019) making it challenging to compare their benefits to more traditional coastal resilience approaches such as seawalls and embankments. Data is a key limiting factor to the understanding of NNBF functions as each site has unique characteristics based on vegetation, geology, and historical context. This produces

challenges when scaling up NNBF studies from one site to a larger region, and yet information at a larger scale would help communities trying to make decisions about whether to implement more NNBF options or more traditional coastal resilience approaches.

Understanding different solutions to reduce the impact of storm surge on the coast is a crucial goal in protecting public safety. The efficiency of vegetated foreshores in reducing wave energy under severe storm conditions is continually being researched (Zhang & Lin, 2020). To address the need for more information on the benefits of NNBF, recent advances in numerical models have parameterized the interaction of the vegetation with hydrodynamics and waves (Anderson and Smith 2014; Ding et al. 2019; DING et al. 2019; Garzon et al. 2018; Jadhav and Chen 2012; Lowe et al. 2007; Marsooli et al. 2017, 2016; Möller et al. 2014; De Oude 2010; Ozeren, Wren, and Wu 2014; A. Rooijen et al. 2020; A. A. van Rooijen et al. 2016; Vuik et al. 2016; Wu et al. 2011; Yang et al. 2012). These studies modeled the "explicit" interactions between waves and vegetation through "site-specific" data on the stem height, stem diameters, and the plant density where they generated the bulk drag coefficient expressions, as a function of Keulegan-Carpenter (KC) or Reynolds (Re), to incorporate the marshes flexible stem characteristic, and to yield a more accurate representation of the attenuation of waves (Jacobsen et al., 2019). This "site-specific" data provides the vegetation characteristics for these studies, but it also limits the extrapolation to larger geographic domains of the explicit interaction of waves and vegetation. There are national vegetation datasets for plant species, such as United States Department of Agriculture (USDA, 2021) that provide the plant species stem growth

height, but it lacks information on the plant density, and stem diameter. This has led to other studies that applied another approach in characterizing the vegetation in numerical models, using an "implicit" representation through equivalent bottom roughness length that is directly correlated to land cover datasets (Nowacki et al., 2017). Studying this implicit interaction allows for the extrapolation of wave attenuation calculation to larger geographical scales to observe the potential benefits of the NNBFs through national landcover datasets, such as the National Landcover Dataset (NLCD, Jin et al., 2019) or the National Wetlands Inventory (NWI, Wilen & Bates, 1995). One such study that employed these approaches studied the difference between the implicit and explicit vegetation in a numerical model to field observations in a marsh (Baron-hyppolite et al., 2018). This study concluded that the implicit interactions of the waves and vegetation did not accurately represent the observations, while the explicit interaction accurately captured the observations. However, this study did not answer if the implicit approach attenuated the waves within the marsh width and how accurate can two spatially different models evaluate the wave and vegetation interactions.

Objective

To further fill this gap, this study focuses on two different marshes in the Chesapeake Bay to investigate: 1) the fidelity of the implicit and explicit representation of vegetation, and 2) the accuracy of numerical models at varying geographical domains in illustrating the wave attenuation by vegetation. The geographical domains employed in this study transpire at a site-specific domain or local scale, and a regional domain or regional scale that is bounded for the United States East Coast. The Chesapeake Bay, located in the mid-Atlantic

coast of the United States, contains around 1.5 million acres of coastal wetlands (Chesapeake Bay Program, 2018) providing opportunities for many unique studies on these complex and productive ecosystems (Hladik et al., 2013) and therefore it is ideally suited for a regional scale wave attenuation model that includes vegetation. At both marsh sites in the Chesapeake Bay, the explicit vegetation approach has been thoroughly studied by comparing a modified numerical model and extensive field observations (Garzon et al., 2018) demonstrating the accuracy of the explicit representation with less than a 20% relative bias compared to field observations. Furthermore, to explicitly represent vegetation at a larger domain there is a need for scaled up vegetation data, but with this lack of data presently the implicit representation is the only viable way to scale up wave attenuation to vegetation.

To represent wave attenuation by marshes, this study compared two different numerical models that can be applied at different geographical scales: a local scale model which is a site-specific domain, and a regional model that has a domain of the United States east coast. The fundamental idea is that scaling up results from field sites could be much simpler if one or both of the following two ways could provide accurate wave attenuation: (1) if plant characteristics can be replaced by a friction parameter, or (2) if regional scale modeling can accurately represent wave attenuation by vegetation.

Therefore, the main question this study seeks to answer is, “What are the trade-offs of different vegetation representations in a numerical model at varying geographical domains?”. To do this, first, a regional model was developed utilizing a coupled hydrodynamic and a phase averaged nearshore wave model for the Chesapeake Bay, where

wave dissipation was modeled in one of two ways: (1) implicit, wave dissipation is modeled using a coefficient of friction; or (2) explicit, wave dissipation is modeled using specific vegetation height, diameter, and density characteristics measured at 2 field sites in the Chesapeake Bay. The regional and local models were then calibrated and validated with hydrodynamic and wave measurements of several Hurricanes that were measured at 2 field sites in Virginia. Then the different numerical models' results were compared in terms of the wave transformation within the marsh to the field measurements at the peak of the storm event. Lastly, evaluation of the schemes employed by the numerical models were compared during different conditions measured in the field throughout the storm events to determine the efficacy of the schemes in representing wave attenuation by vegetation.

CHAPTER TWO: METHODOLOGY

This study is based on a comparison between field campaigns that measured hydrodynamic, waves, vegetation characteristics, and topo-bathymetric conditions and numerical modeling in two natural marsh areas within the Chesapeake Bay. The study sites were located in two natural reserves located in the southern tip of the Delmarva Peninsula in Virginia, the Eastern Shore of Virginia National Wildlife Refuge and Magothy Bay Natural Area Preserve (Figure 1). Magothy Bay Natural Area Preserve is approximately 500m from the coastline to the end of the marsh where a levee has been established preventing encroachment of waves and water levels. It also has a channel that extends from the bay where it branches off to other parts of the marsh. The Eastern Shore of Virginia National Wildlife Refuge is located behind an inlet created by the barrier island system that runs along the Delmarva Peninsula and the Fisherman Island National Wildlife Refuge. This marsh has an approximate distance 375m from the water to the end of the marsh with a channel that extends from the water where it branches off to other parts of the marsh. Both sites are dominated by the smooth cordgrass, *Spartina alterniflora.*

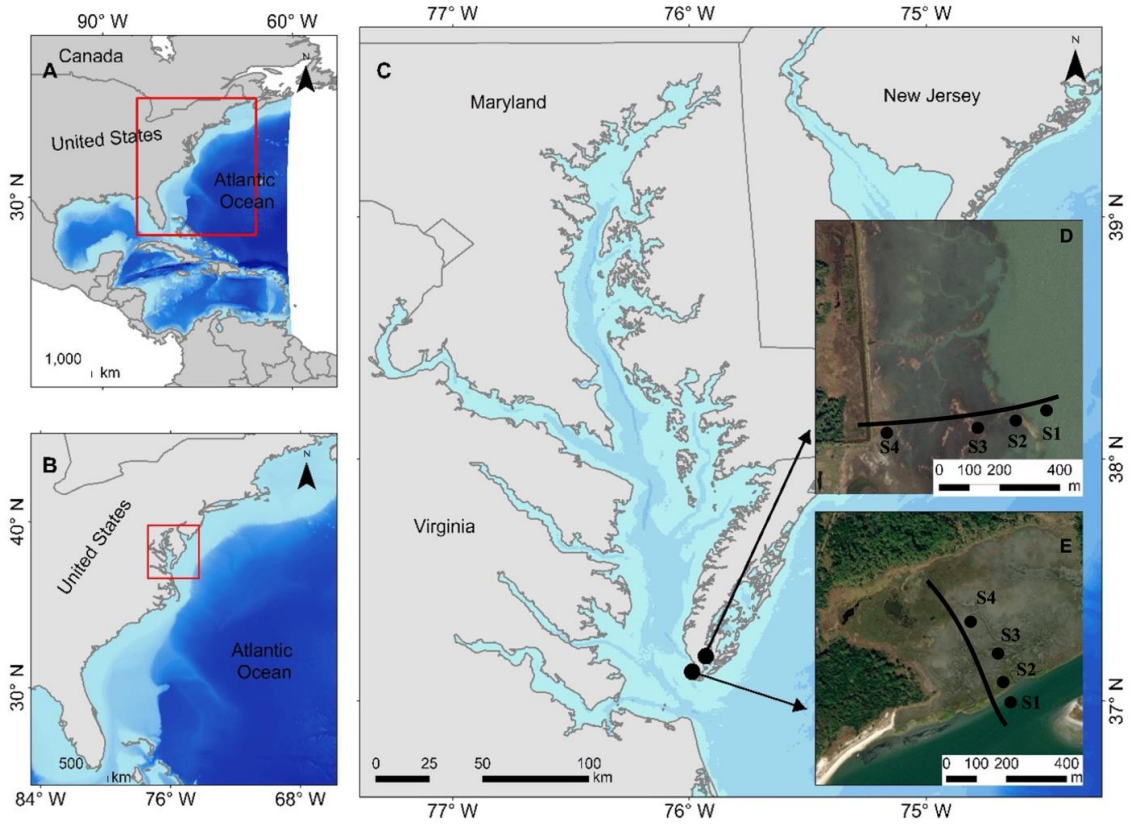

Figure 1 Location map of the study site. C) Chesapeake Bay Region with points representing the study sites in the south. D) Magothy Bay Natural Area Preserve that show the observation stations. E) Eastern Shore of Virginia National Wildlife Refuge that show the observation stations.

2.1 Field Measurements

In order to implement the regional and local numerical models at each study site and evaluate their performance, the field observations include hydrodynamic and wave measurements, vegetation characteristics, and nearshore topo-bathymetric surveys. A shallow-water bathymetric survey and a high-resolution topographic survey were performed for each site covering the marshes, and the submerged beach using a differential GPS Trimble R4 (error lower than 0.02 m in elevation) and from the corrected data, a 1 m-

cell digital elevation model (DEM) was computed. The vegetation measurements were collected at each of the observation stations in Figure 1. These surveys reported the various vegetation species and characteristics (stem height, stem diameter, and plant density) along the marsh platform (Paquier et al., 2017).

To measure the hydrodynamics and waves a range of high-frequency pressure transducers (Trublue Measurement Specialties) deployed at each station along each transect. These sensors record pressure continuously at 4 Hz. The measured total pressure data consisted of the combination of hydrostatic pressure, dynamic wave pressure, and atmospheric pressure. In order to calculate the significant wave height from the pressure, the following procedure was taken: 1) A time-domain analysis of the dynamic pressure, where the dynamic pressure components are separated and then the data is cut into bursts of 4800 sample measurements; 2) to reduce uncertainties produced by the time domain analysis, a frequency domain analysis is then applied to solve for the wave spectrum with MATLAB's Fast Fourier Transforms with parameters of 1024 components and 20-min Hanning windows with 75% overlapping in each burst; 3) Solving for the area under the wave spectrum, the Zero Moment (Hm0) wave height can be calculated by (Kamphuis, 2010):

Equation 1: Zero Moment Wave Height

$$H_S \approx H_{m0} = 4\sigma_f$$

where σ_f is the standard deviation of the water surface elevation calculated from the frequency analysis, and H_S(m) is the significant wave height. This provided the approximate significant wave height (Hs) at each field site. In Table 1, it shows the storms measured at the 2 study sites in the Chesapeake Bay.

Table 1: Recorded Data

Sample	Storm	Year	max hm0 at S1 [m]	max surface water at S1 [m above ground]	Topography/Bathymetry	Vegetation
Eastern Shore of Virginia National Wildlife Refuge	Hurricane Joaquin	2015	0.3754	1.8	TRUE	h_v,b_v,N_v
Magothy Bay Natural Area Preserve, Virginia	Hurricane Jose	2017	0.3618	2.054	TRUE	h_v,b_v,N_v

During the period of data collection, two Hurricanes were recorded, Hurricane Joaquin (2015) at Eastern Shore and Hurricane Jose (2017) at Magothy Bay. The high-frequency pressure sensors collected roughly 3 days before the storm impact and 5 days after the storm impact.

Hurricane Joaquin (Berg, 2016) formed outside of the tropical areas in the Atlantic Ocean. This cyclone moved over warmer waters and intensified rapidly to become a hurricane in the east of the San Salvador Island on the 1st of October 2015. The storm continued to strengthen reaching the category 4 on the 2nd of October. By the 3rd of October, the hurricane accelerated northeastward away from the Bahamas. Late on 4th and 5th of October, the cyclone moved north northeastward over the Atlantic Ocean, and on 6th and 7th, Hurricane Joaquin became embedded itself off the mid-Atlantic coast. Since it was off the coast there was no severe storm surge flooding in the USA directly attributed to this cyclone, but high tides, onshore winds behind a frontal boundary and swells propagating away from Hurricane Joaquin. Flooding occurred in South Carolina, North Carolina, and

Virginia, where maximum storm surge reached 1.25m and 1.18m at Money Point NOAA station and Chesapeake Bay Bridge Tunnel NOAA station.

Hurricane Jose (Blake, 2015) first formed as a thunderstorm off the west coast of Africa on 31st of August. After its formation, Jose started moving westward to west-northwestward across the Atlantic Ocean by the 9th of September, steered by a mid-tropospheric ridge located to its north. Then by September 12th, Jose became trapped near a large cyclone, Hurricane Irma, and causing Jose to slow down and make a clockwise loop in the southwestern Atlantic through 16 September. With a surge of colder air intensifying Hurricane Jose for 5 days then it started to weaken to a tropical storm where it moved northward, but it began to wander up the coast of southeastern New England on 21 September. There was minor coastal flooding from Hurricane Jose in the mid-Atlantic region with a surge reaching 1.25m in Chesapeake Bay Bridge Tunnel NOAA station and 1.48m at the Wachapreague, VA station.

2.2 Numerical modeling

The numerical models employed at the varying geographical scales in this study involved a local scale high-resolution numerical model XBeach (Roelvink et al., 2009) and a regional scale coupled ADCIRC-UNSWAN. XBeach uses the Generalized Lagrangian Mean (GLM) formulation (Andrews & Mcintyre, 1978) of the shallow water equations and a time-dependent version of the wave action balance equation (Holthuijsen et al., 1989). For this study XBeach is employed only using the hydrodynamics to be adapted for coastal salt marshes to calculate the interaction of waves and vegetation. The coupled Advanced

CIRCulation model (ADCIRC) and Simulating WAves Nearshore (SWAN) simulates the water level by solving the generalized wave continuity equation (GWCE) and currents by using the vertically integrated shallow water equation (Westerink et al., 2008) with the wave model solving a Eularian, phase-averaged, refraction model (Booij et al., 1999), provides wave propagation in irregular bathymetry and topography (Gorrell et al., 2011).

2.2.1 Model implicit and explicit formulations for wave attenuation by vegetation

The numerical models calculate the wave attenuation by vegetation through two different formulations: (1) explicit, or (2) implicit. The numerical models SWAN and XBeach represent the wave interaction to vegetation through an additional term in the wave action balance equation (Holthuijsen et al. 1989) to represent the wave attenuation processes by vegetation, in addition to the wave attenuation by bottom friction. The total wave energy dissipation by vegetation (A. A. van Rooijen et al., 2015) is taken into account in XBeach and SWAN by solving the wave action balance in Equation 2 where $A = \frac{E_W}{\sigma}$, $E_W(\frac{Nm}{m^2})$ is the wave energy, σ is the intrinsic wave frequency, $D_{break}(\frac{W}{m^2})$ is the wave dissipation due to break, $D_{veg}(\frac{W}{m^2})$ is the wave dissipation to vegetation, $D_f(\frac{W}{m^2})$ is the wave dissipation to friction, lastly $c_g(\frac{m}{s})$ is the wave propagation speeds for (x, y, θ) space.

Equation 2: Short Wave Action Equation

$$\frac{\partial A}{\partial t} + \frac{\partial c_{g,x} A}{\partial x} + \frac{\partial c_{g,y} A}{\partial y} + \frac{\partial c_{g,\theta} A}{\partial \theta} = -\frac{D_{break} + D_{veg} + D_f}{\sigma}$$

Equation 3: Total Wave Energy Dissipation by Vegetation

$$D_{veg,i} = A_v * \frac{\rho \widetilde{C}_{D,i} b_{v,i} N_{v,i}}{2\sqrt{\pi}} \left(\frac{kg}{2\sigma}\right)^3 H_{rms}^3, \text{ with}$$

$$A_v = \frac{(\sinh^3 k\alpha_i h - \sinh^3 [\![k\alpha_{i-1} h)]\!] + 3(\sinh k\alpha_i h - \sinh k\alpha_{i-1} h)}{3k\cosh^3 kh}$$

The total attenuation by vegetation, D_{veg} $(\frac{W}{m^2})$, is solved in Equation 3 where h is the water depth, H_{rms}(m) is the root mean square wave height, k is the wave number, $\widetilde{C}_D$ is the bulk drag coefficient, b_v(m) is the vegetation stem diameter, $N_v(\frac{\#\ of\ stems}{m^2})$ is the vegetation density, and α is the relative vegetation height $\left(= \frac{h_v}{h}\right)$ for layer i. The implicit formulations for wave attenuation due to vegetation is solved in the wave action balance and in order to solve the Dissipation by friction the friction length is solved first in Equation 4.

Equation 4: Nikarudse Friction Length

$$K_n = Hexp\left[-\left(1 + \frac{kH^{\frac{1}{6}}}{n\sqrt{g}}\right)\right]$$

Equation 5: Nondimensional Friction Factor

$$\frac{1}{4\sqrt{f_w}} + \log\left(\frac{1}{4\sqrt{f_w}}\right) = m_f + \log\left(\frac{a_b}{K_n}\right), \text{ with } a_b^2 = 2\iint \frac{1}{\sinh^2 kh} F(f,\theta) df d\theta$$

Equation 6: Madsen Bottom Friction Equation

$$C_b = \frac{f_w g}{\sqrt{2}} U_{rms}$$

Equation 7: Total Dissipation by Friction

$$D_f = -C_b \frac{\sigma^2}{g^2 \sinh^2 kd} E(\sigma,\theta)$$

where the bottom friction length is K_n(m), n is the Mannings' value, H(m) is the wave height, and $g(\frac{m}{s^2})$ acceleration of gravity. Then after solving for the bottom friction length, the nondimensional friction factor can be calculated in Equation 5, where the f_w is the nondimensional friction factor, m_f is a constant (Jonsson & Carlsen, 1976), a_b is the near bottom excursion amplitude, h(m) is the water depth, and k is the wave number. Then the bottom friction coefficient is solved, where $U_{rms}(\frac{m}{s^2})$ is the bottom orbital motion. Finally, the total wave attenuation due to bottom friction is derived in Equation 7. In the numerical models, the vegetation represented implicitly through the attenuation of bottom friction is treated as an enhanced bottom friction value, made to represent the increase resistance that occur when the waves interact with the saltmarsh.

2.2.2 Regional Model Development

The Regional model was created with a domain that extends from the northern parts of Venezuela to Nova Scotia (shown in Figure 2). The domain of the regional numerical model was to capture the wave propagation provided from the Hurricanes as it traveled through western Atlantic Ocean. The resolution of the model in the ocean varies from 50 to 75 km with a resolution of 2.5 km along the coast. In the Chesapeake Bay the model is further resolved with resolution varying from 100m to 500m and at the field sites. Lastly, for the field sites the mesh was developed to have higher resolutions that reach an estimated 15m. The Regional model's unstructured grid was developed using the MATLAB library

OceanMesh2D (Roberts et al., 2019) for varying bathymetry and topography data sources. The bathymetry and topography have been assembled from: GEBCO (Weatherall et al., 2015), National Oceanic and Atmospheric Administration (NOAA) Coastal Relief Model (Blanton et al., 2011), United States Geological Survey (USGS) Coastal National Elevation Database (Danielson et al., 2016), and field measured elevation datasets. The topography and bathymetry was then transformed to the vertical datum North American Vertical Datum 1988 (NAVD88) using NOAA's vertical datum transformation tool, VDATUM (White, 2007).

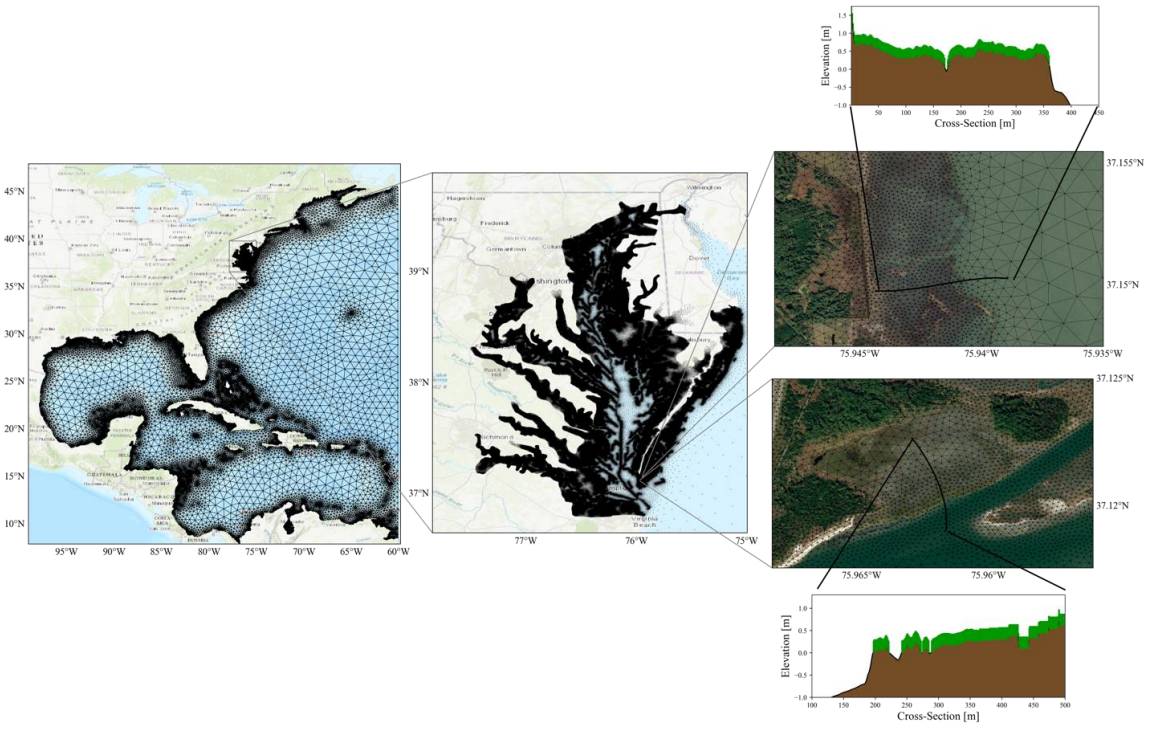

Figure 2 Regional Model. (Left) Domain of the Finite Element Mesh. (Middle) Higher resolution within the Chesapeake Bay with a max resolution of 150m. (Right) Study sites high resolution reaches 15m and the 1D cross sections for the local numerical model.

For the regional model attributes, the Manning's *n* friction length was determined based on the National Land Cover Database (NLCD) 2016 (Jin et al., 2019), shown in figure 3, where the classes Herbaceous and Woody wetlands varied in Manning's *n* from the minimum of the range 0.045, to a median of 0.080, and a maximum value 0.150 based on the manning's *n* classes from in Ferreira et al., 2014. To avoid affecting the hydrodynamics in the numerical model, it was decided to separate the bottom friction impacting the hydrodynamic equations from the wave action balance in the coupled ADCIRC-SWAN model, which was implemented by creating a new attribute "swan_frict". Another new attribute was introduced to the regional model, "swan_nplant", which was manually implemented based on the field site locations. For each site, the vegetation height, diameter, and density were implemented from the data collection in the field discussed earlier. The bulk drag coefficients were decided based on studies with similar hydrodynamic conditions and vegetation types (Garzon et al. 2019; Jadhav and Chen 2012; Smith et al. 2016). In Garzon et al. 2018, the numerical model was modified to calculate the bulk drag coefficient during the simulation, instead of being inputted as a constant value, but for this study the bulk drag coefficient is held constant to have an accurate comparison to the regional model. This led to the decision of using bulk drag coefficients with values of 1, 2, and 3 to capture the full range of the *Spartina alterniflora*.

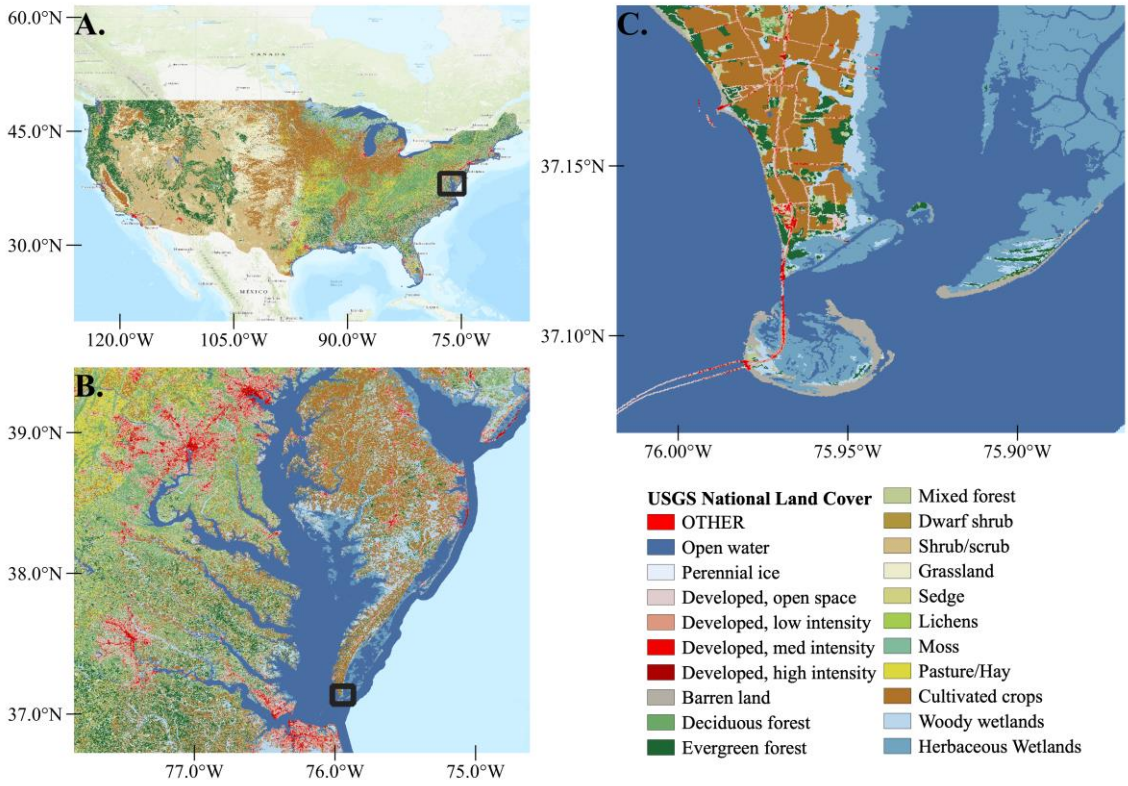

Figure 3 National Landcover Dataset 2016. (A) Landcover of the United States. (B) Landcover in the Chesapeake Bay Domain. (C) Landcover at the Study sites.

The Hurricane forcings generated for Hurricane Joaquin used wind and pressure fields from the European Center for Medium-Range Weather Forecasts (ECMWF) guided by the findings in Garzon et al., 2018. The current ECMWF atmospheric circulation model is ERA 5 (Tarek et al., 2019; Vitart et al., 2019) with a resolution of 0.5 decimal degrees. However, for Hurricane Jose, ERA 5 was unable to simulate the surge and wave heights at the field sites prompting an additional forcing with the atmospheric model from the National Centers of Environmental Prediction (NCEP) was used, the climate forecast

system version 2 (CFSv2, Saha et al. 2014). From these models, the wind at 10 meters above the ground and pressure at mean sea level was extracted to force the ADCIRC-SWAN model.

2.2.3 Local Model Development

The local model was developed using the Delft3D graphical user interface with varying resolution from 10m to 1m. The model incorporates the same topography and bathymetry as the regional model discussed earlier, cross sections are shown in figure 2 for the study sites. The numerical model is set up for a 1 dimensional cross section in 'surf beat' mode, where the short-wave motion is solved using the wave action equation (A. A. van Rooijen et al., 2015). Furthermore, any process related to sediment transport and seabed changes was neglected and the cross-shore profile was kept invariable throughout the simulations. The wave breaking model described by (Daly et al., 2012; Roelvink et al., 2009) was used and all parameters in the model were kept by default. The simulations were performed over a varying spatial resolution profile, with a minimum resolution of 1 m. The offshore water levels boundary conditions were based on the regional model simulation results, that were forced with either ERA5 or CFS, before the marsh site. Wave boundary conditions, applied using a JONSWAP spectrum, were defined also based on the data from the regional model at the same location, which is not affected by breaking and vegetation-induced dissipation. While the model also allows considering a strong vertical variation in the plant characteristics (e.g. mangroves), although, in this study, the *Spartina alterniflora* are considered vertically uniform.

2.3 Model evaluation

To calibrate and validate the models under the observed events at the study sites, the following storm events are evaluated: Hurricane Joaquin 2015, and Hurricane Jose 2017. Table 2 identifies the implicit and explicit configurations implemented in each model. Each storm was simulated through 6 different regional model configurations that were defined above: 3 explicit, and 3 implicit. The local model was simulated for each Hurricane with 3 explicit configurations as well, but the domain on the local model limited the propagation of the measured Hurricane events for this reason a one-way coupling to the regional model's implicit 0.045 at the local model's boundary in the open water to provide wave heights and hydrodynamics.

Table 2: Model Parameters

Storm Event	Numerical Model	Implicit Representations	Explicit Representations			
			Stem Height (m)	Stem Diameter (m)	Plant Density (stems per m^2)	Bulk Drag Coefficient (C_D)
Hurricane Joaquin (2015)	Regional	[0.045, 0.080, 0.150]	0.71	0.00534	344	[1, 2, 3]
	Local	-	0.71	0.00534	344	[1, 2, 3]
Hurricane Jose (2017)	Regional	[0.045, 0.080, 0.150]	0.51	0.00534	453	[1, 2, 3]
	Local	-	0.51	0.00534	453	[1, 2, 3]

Validation of the regional model to the field data recorded at station 1 (Figure 1), located in the water before the marsh, by comparing to the observed time-series, then calculating

the root mean square error (RMSE) of the time series comparison before performing further analysis within the marsh.

The regional and local models were compared to the observations further in the marsh for the H_S at the peak of each storm. The H_S was converted into a percentage by dividing the H_S at station 1 to the H_S propagating in the marsh. Then to determine the wave attenuation coefficient, based on linear wave theory in equation 8 following Bouma et al., 2010, analyzed the peak of each storm.

Equation 8: Wave Attenuation Coefficient from Linear Wave Theory

$$\frac{1}{H_x} = \frac{1}{H_0} + \alpha(x - x_0)$$

with H_0(m) and H_x(m) being the wave heights at the given locations x(m) and x_0(m), and α(m^{-2}) the wave attenuation coefficient. To compute the error of the models to the observations the relative bias was calculated. Finally, in order to determine the difference between the 2 schemes and the 2 geographical scaled models the wave attenuation distance was evaluated. The wave attenuation distance was determined by the length at which the wave attenuation goes to 0 from the edge of the marsh.

Furthermore, in order the explore the behavior of the regional and local models under varied hydrodynamic and wave conditions, a number of hydrodynamic and waves conditions were defined by the field measurements. This analysis was defined at 3 different water levels and 3 different wave heights that were measured at each study site (Table 3). The different water level conditions were defined as such: the low water level, when the marsh was still considered “wet”, the medium water level, when the measured water level

is at its highest, but the vegetation is still emerged, and the last water level was the highest water level recorded at the field sites where the vegetation was submerged. These conditions followed the same procedure as the peak storm analysis where the comparison between observations over the cross section, the relative bias to the observations, and the attenuation length. The wave attenuation length for the conditions shows the best implicit and explicit scheme for the regional and local models.

Table 3: Water Level and Wave Height Conditions

Site	Conditions	Water level [m at NAVD88]	Hs [m]
Eastern Shore	Low, Low	0.28	0.12
Eastern Shore	Low, Medium	0.28	0.22
Eastern Shore	Low, High	0.28	0.31
Eastern Shore	Medium, Low	0.61	0.14
Eastern Shore	Medium, Medium	0.61	0.21
Eastern Shore	Medium, High	0.61	0.28
Eastern Shore	High, Low	0.82	0.1
Eastern Shore	High, Medium	0.82	0.22
Eastern Shore	High, High	0.82	0.32
Magothy Bay	Low, Low	0.51	0.10
Magothy Bay	Low, Medium	0.51	0.18
Magothy Bay	Low, High	0.51	0.22
Magothy Bay	Medium, Low	0.73	0.15
Magothy Bay	Medium, Medium	0.73	0.23
Magothy Bay	Medium, High	0.73	0.37
Magothy Bay	High, Low	0.98	0.20
Magothy Bay	High, Medium	0.98	0.28
Magothy Bay	High, High	0.98	0.42

CHAPTER THREE: RESULTS

3.1 Numerical Model Validation

Observation data for the sensor in the water (Station 1) before the marsh edge was used to validate the numerical model prior to evaluating the inland propagation of waves. Hurricane Joaquin was first validated against observations (Figure 4) for the H_S and water levels at the marsh edge. The water levels for Hurricane Joaquin had an RMSE < 8.65cm, while the significant wave height had an increased RMSE < 12.79cm. The model overestimates the peak wave height by 5 cm, while the water surface elevation shows a good fit to the observed surge at Eastern Shore.

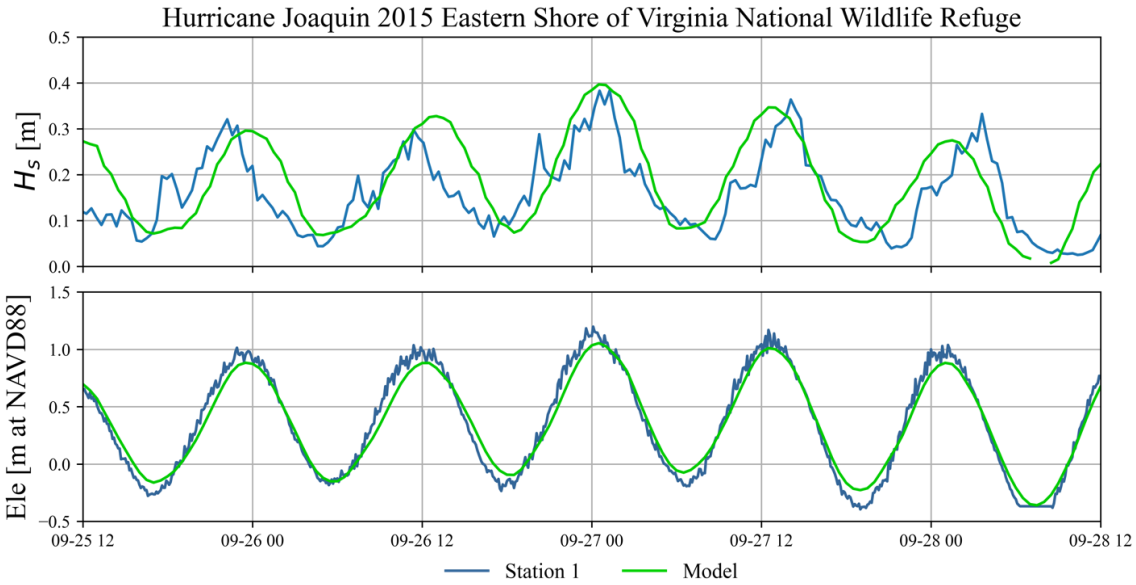

Figure 4 Hurricane Joaquin 2015 field and model comparison. (Top) Comparison of modeled wave height and observations at station 1. (Bottom) Comparison of modeled water level and observations at station 1.

The regional model was then validated for Hurricane Jose 2017 where the observations were compared to the model (Figure 5). The analysis of the observed and modeled water levels shows that the model has an RMSE < 22cm. While the modeled H_S have an RMSE < 9.6 cm. It shows the model is underestimating the peak wave height by 2 cm at station 1 in Magothy Bay. The water levels for station 1 are showing an underestimation during the high tide and overestimation in the lower water levels, however, greater agreeability is seen during the surge on 2017-09-19.

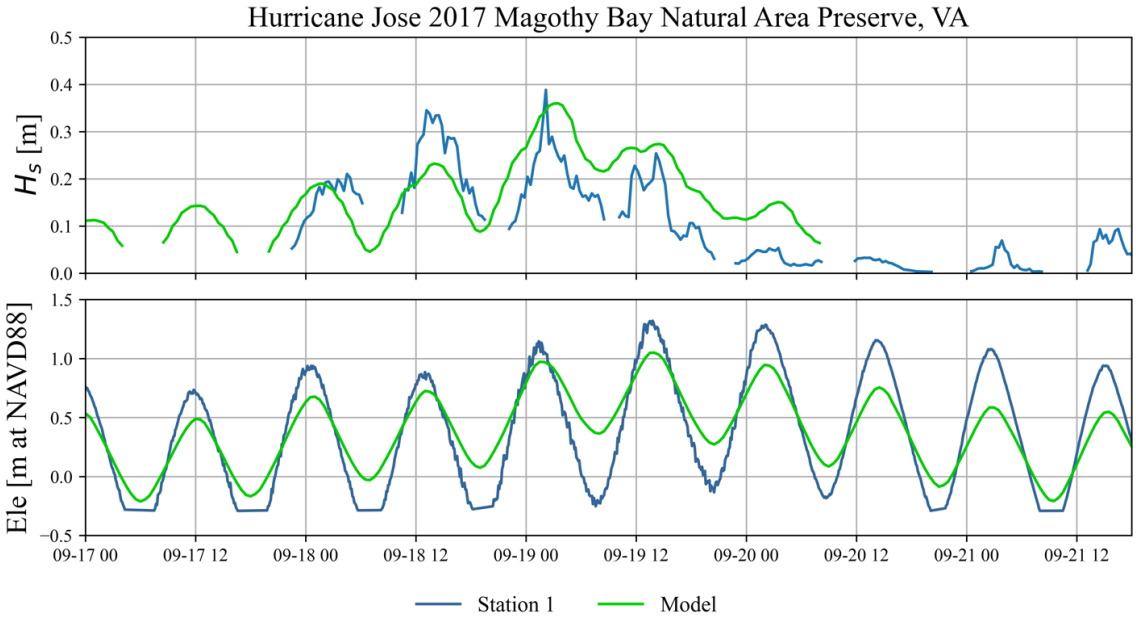

Figure 5 Hurricane Jose 2017 field and model comparison. (Top) Comparison of modeled wave height and observations at station 1. (Bottom) Comparison of modeled water level and observations at station 1.

3.2 Wave Attenuation

After the model was validated, analysis of the modeled wave heights that propagated in the marsh to compare the observed wave heights as a function of distance. In Figure 6, the H_S

starts at 100% at station 1 at both sites, as the wave heights are not affected by the dissipation of the marsh. At the edge of the marsh, the H_S modeled by the varied schemes start diverging. At Eastern Shore, during Hurricane Joaquin, the regional implicit schemes at station 2 start to show an underestimation of ~20% of the wave attenuation, while the explicit schemes, for both regional and local models, maintain less than a 10% bias compared to the observations. At Station 3, the implicit schemes further underestimate the wave attenuation by more than a 40%. The regional model explicit scheme with a C_D=1 and the local explicit C_D=1 stayed within a 5% bias to the observations. At station 4, the regional implicit schemes continue to underestimate the wave attenuation with ~30% difference, while the explicit schemes, for regional and local, are within 10% difference to the observations. For the second site, Magothy Bay, at station 2 showed that the regional and local models for all schemes performed with a 5% difference to the observations. At station 3, the schemes start diverging up to 20% for the regional implicit schemes, while the regional explicit scheme C_D=1 stays within a 7% difference. The local explicit C_D=1 performs the best with a bias of 1.74% to the observations. At the final station in Magothy Bay, station 4 that is 450m from the edge of the marsh, shows the wave height attenuation for the regional implicit schemes show reduction in differences with a bias ~20%, and the explicit models, for both regional and local, show close to full attenuation with the regional explicit C_D=2 performing best at a bias of less than 1%.

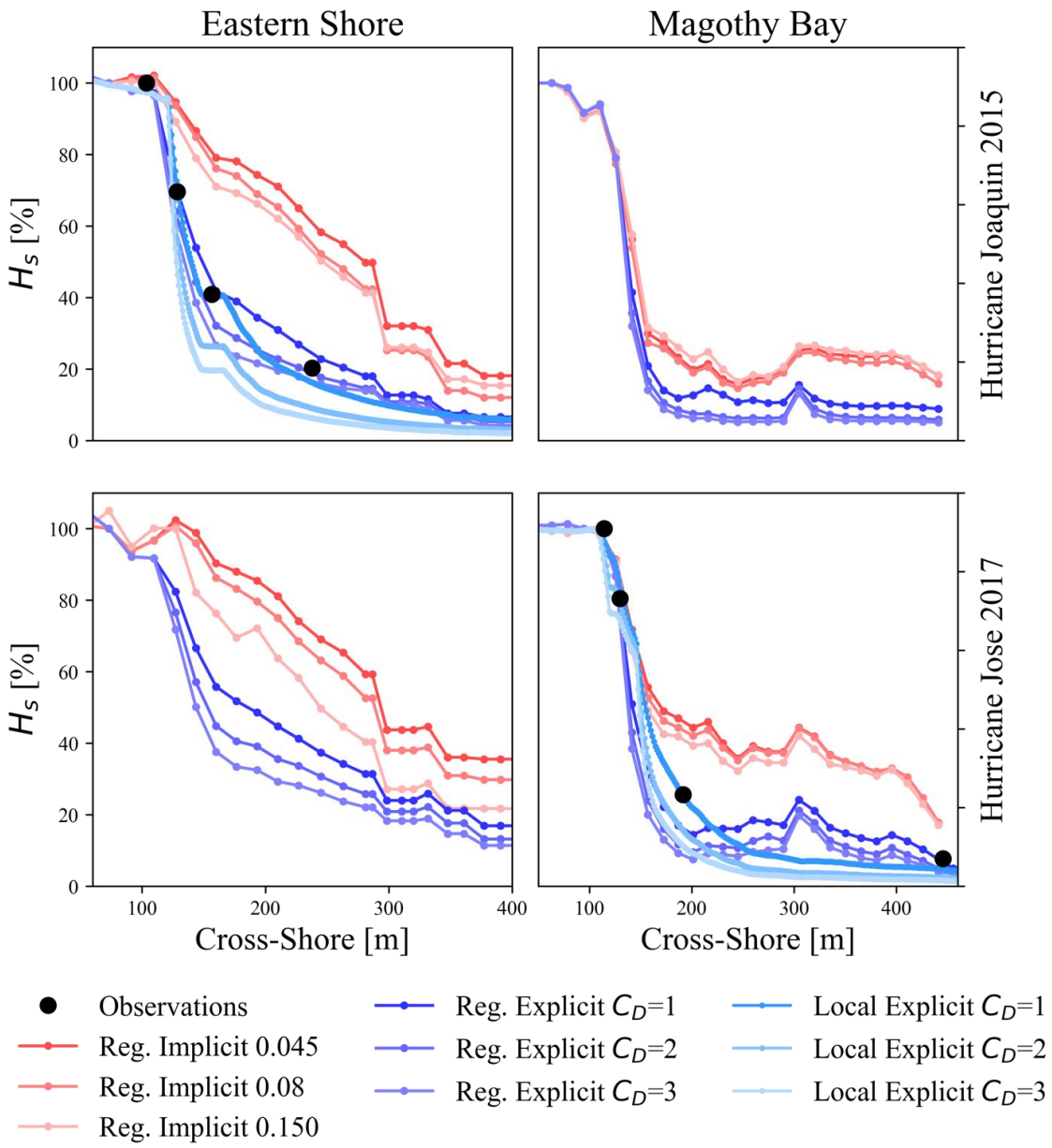

Figure 6 Wave Height as a function of distance for each site at the peak of the Hurricanes. Observations for Hurricane Joaquin at Eastern Shore, and for Hurricane Jose at Magothy Bay.

The wave height attenuation coefficient was calculated throughout the marsh length (Figure 7). For both sites, figure 7 shows the calculated wave attenuation coefficient with the observations having an average attenuation coefficient of 0.046 at Eastern Shore and

0.184 at Magothy Bay. Eastern Shore the attenuation coefficient increases as the distance increases into the marsh for all schemes, but the regional implicit shows a large difference in the attenuation due to vegetation. The regional implicit schemes start to diverge with the increasing friction getting closer to the observation's coefficient at station 4. The regional explicit and local explicit both show similar attenuation coefficients to the observations for stations 2 and 3, while the local models C_D=2 and C_D=3 show overestimation in the coefficient at station 4. At Magothy Bay the attenuation coefficients follow a similar trend to the Eastern Shore site, however the magnitude of attenuation coefficient has significantly increased. The regional implicit schemes show some diverging at station 3 with a difference between each scheme of 0.05. The explicit schemes, both the regional and local, show overestimation in the coefficient at station 3 and 4, but the local explicit C_D=1 accurately matched the observed coefficients.

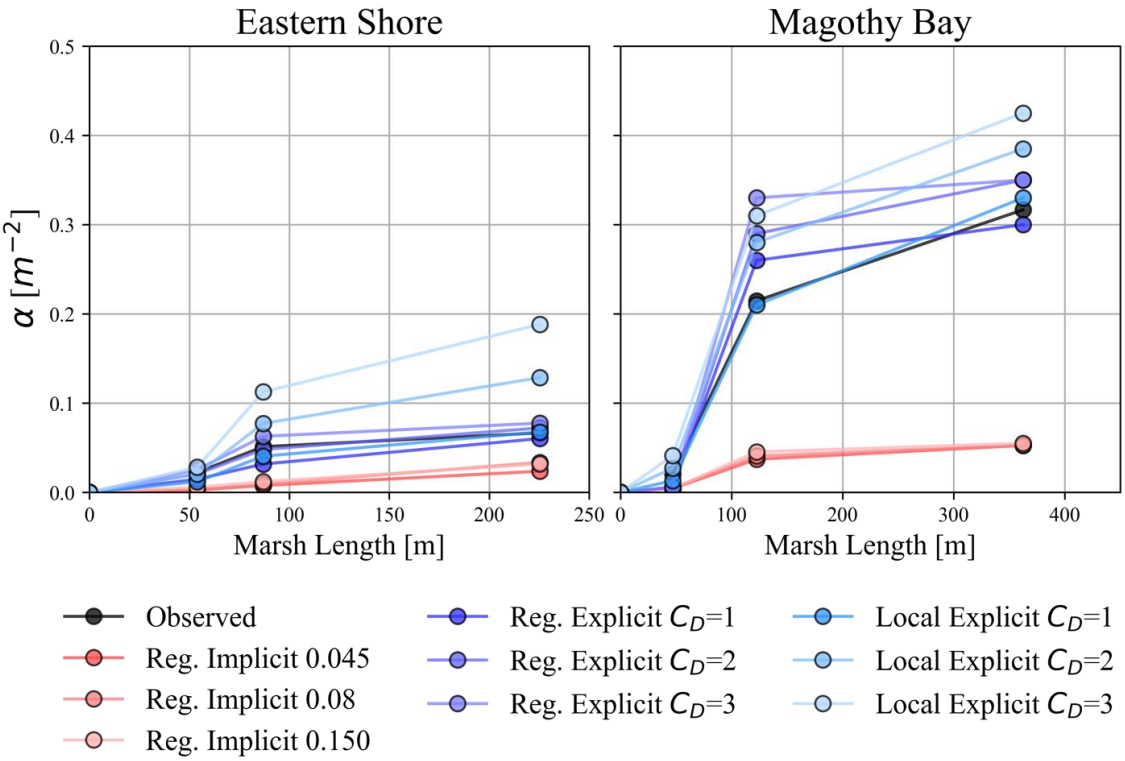

Figure 7 Wave attenuation by vegetation (as α) as a function of distance. (Left) Eastern Shore Wave Attenuation Coefficient over the distance of the marsh. (Right) Magothy Bay Wave Attenuation over the distance of the marsh.

At each site, the relative bias was calculated and is shown in Figure 8 and in Table 4 for all schemes. Eastern Shore station 1 exhibited no differences between the observations and the schemes. The waves propagated toward station 2, located 4m from the edge of the marsh, the local explicit C_D=1 accurately captured the observations, while the regional implicit schemes underestimated the attenuated wave height and the regional explicit C_D=2 and C_D=3 slightly overestimated the attenuated wave heights. At stations 3 and 4 the schemes diverged further with the regional explicit schemes capturing the attenuated wave heights while the local explicit C_D=1 slightly underestimated the attenuation and C_D=2 and C_D=3 overestimated the attenuation. The regional implicit schemes highly underestimated

the wave attenuation with the regional implicit 0.15 performing slightly better than the other frictions. Magothy Bay station 1 exhibited no differences since there has been no interaction to the vegetation in the marsh. At station 2 located at the edge of the marsh, there is little to no differences between the schemes with the local explicit C_D=2 performing the best and the other local schemes either slightly underestimated or slightly overestimated the wave attenuation. The regional explicit schemes consistently underestimated the wave attenuation, while the regional implicit schemes underestimated the attenuation 5% more than the regional explicit schemes. At stations 3 and 4, the schemes show further divergence to the observations. Starting at station 3 the local explicit C_D=1 performing the best while the other local schemes overestimated the attenuation. The regional implicit schemes underestimated the attenuation by another 15%, while the regional explicit schemes overestimated the attenuation similarly to the local explicit C_D=2 and C_D=3. At station 4 the explicit schemes, regional and local, show full attenuation with some slight overestimations, but the regional implicit schemes further underestimated the attenuation with little difference between the varying frictions.

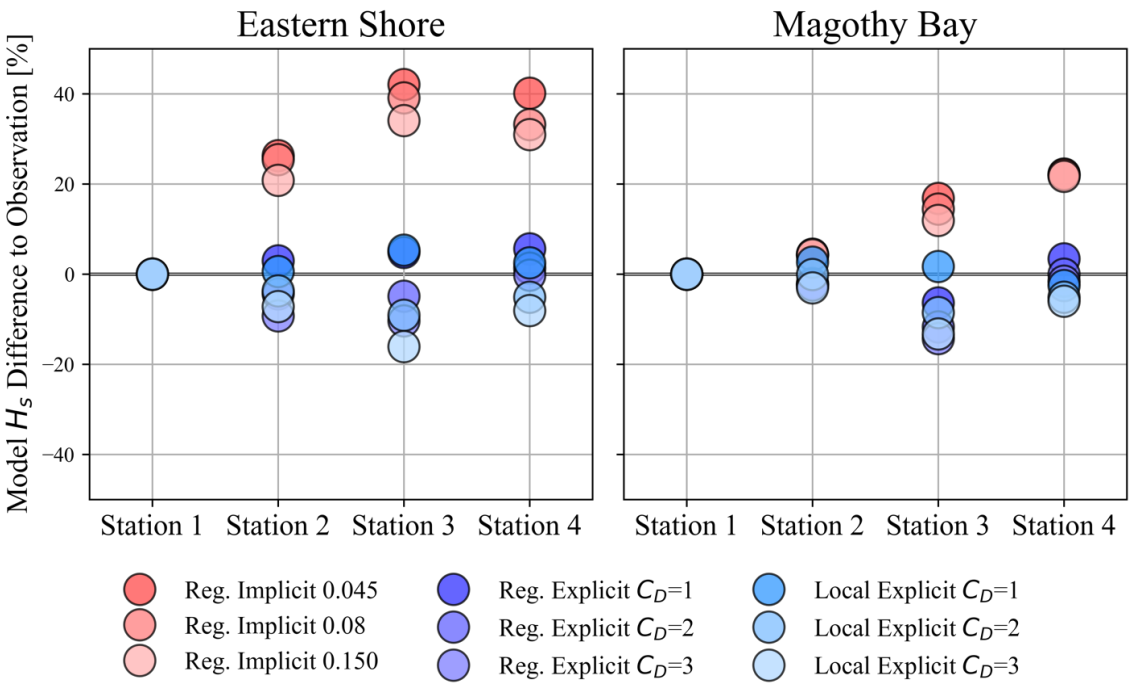

Figure 8 Calculated Wave Attenuation Relative Bias. (Left) Eastern Shore relative bias for each observation station. (Right) Magothy Bay relative bias for each observation station.

Table 4: Calculated Relative Bias

	Eastern Shore				Magothy Bay			
	Station 1	Station 2	Station 3	Station 4	Station 1	Station 2	Station 3	Station 4
Reg. Implicit 0.045	0.00	26.31	42.09	40.11	0.00	10.87	16.80	22.22
Reg. Implicit 0.080	0.00	25.40	39.09	33.20	0.00	10.70	14.45	22.08
Reg. Implicit 0.150	0.00	20.82	34.04	30.96	0.00	9.65	11.92	21.72
Reg. Explicit C_D=1	0.00	2.98	**4.79**	5.61	0.00	4.98	-6.34	3.43
Reg. Explicit C_D=2	0.00	-4.38	-4.86	1.32	0.00	4.90	-11.72	**0.024**
Reg. Explicit C_D=3	0.00	-9.27	-10.38	**-0.21**	0.00	4.82	-14.27	-1.55
Local Explicit C_D=1	0.00	**0.609**	5.34	2.51	0.00	5.099	**1.70**	-2.50
Local Explicit C_D=2	0.00	-3.69	-9.12	-5.13	0.00	**-0.061**	-8.54	-5.136
Local Explicit C_D=3	0.00	-7.21	-16.10	-8.08	0.00	-5.32	-13.23	-6.034

The distance it takes for each scheme to attenuate the waves within the marsh is shown in figure 9. Eastern Shore the regional implicit schemes attenuated waves between 425-480m,

while the regional explicit schemes attenuated the waves 100m earlier within 295-340m in the marsh. The local explicit schemes attenuated the waves the earliest by almost 100m, depending on the drag, to the regional explicit schemes whereas there were further differences to the regional implicit up to 200m. At Magothy Bay, the regional implicit schemes show full attenuation at 480m and could be due to the levee in this marsh. The regional explicit schemes show dramatic differences between the 3 drag schemes with the C_D=1 attenuating 20m earlier then the implicit schemes, C_D=2 attenuates the waves 90m earlier then the implicit, and the C_D=3 attenuates the waves the earliest out of the regional explicit schemes at 200m almost 300m before the regional implicit schemes. The local explicit schemes have similar results to the Eastern Shore site, where C_D=1 attenuated the waves at 260m around 220m earlier then the regional implicit schemes. The local C_D=2 attenuated the waves earlier in the marsh, 220m, extending the difference to the regional implicit schemes by 240m. Lastly, the local explicit C_D=3 attenuated the waves at the same distance within the marsh as the regional explicit C_D=3, 200m.

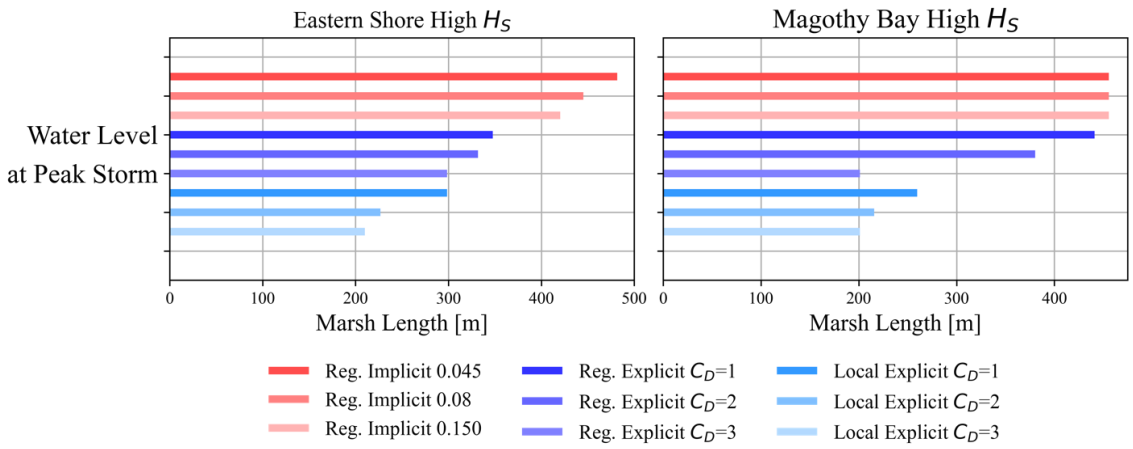

Figure 9 Wave Attenuation Length at each site for the peak of each Hurricane. This is showing the length at which the wave heights go to 0 starting from the marsh edge.

3.3 Implications of Water level and Waves conditions on Attenuation

The water level and wave height conditions measured at the field sites are used to evaluate the influences that the modeled schemes have on the wave attenuation be vegetation.

3.3.1 High Wave Height Conditions

The water level conditions at the high wave heights are shown in Figure 10 as a function of the distance within the marsh. Eastern Shore, the low water condition shows reduced differences between the regional implicit schemes and the explicit schemes. The regional explicit schemes capture the observations and show similarities to the local explicit results. During the medium water level, the differences between the regional implicit schemes and the explicit schemes increases. Similarly, to the low water level the medium water level regional explicit schemes capture the observations along with the local explicit schemes. The last condition for Eastern Shore, the high water level, the difference between the

regional implicit schemes and the explicit schemes show the greatest difference, close to about 30% at stations 3 and 4. The regional explicit schemes capture the observations, while the local explicit C_D=2 and C_D=3 notably overestimate the wave attenuation at stations 3 and 4. Magothy Bay, the low water level shows a small difference between the regional implicit and the explicit schemes, except for a dynamic showing between station 3 and 4 when the regional implicit schemes show a sudden decrease in the wave attenuation. During the medium water level condition, the results show an increase difference between the regional implicit schemes and the explicit schemes starting a little before station 3 and throughout to station 4. The regional schemes accurately predict the wave attenuation at both station 3 and 4, but the local explicit C_D=1 slightly underestimates the wave attenuation at station 3. For the final condition, the high-water levels at Magothy Bay, the difference increases further between the regional implicit schemes and the explicit schemes close to 30%. The regional explicit C_D=1 predicts the wave attenuation to the observations while C_D=2 and C_D=3 slightly overestimate the attenuation at station 3. The local explicit schemes C_D=2 and C_D=3 predict the attenuation whereas C_D=1 underestimate the attenuation at station 3.

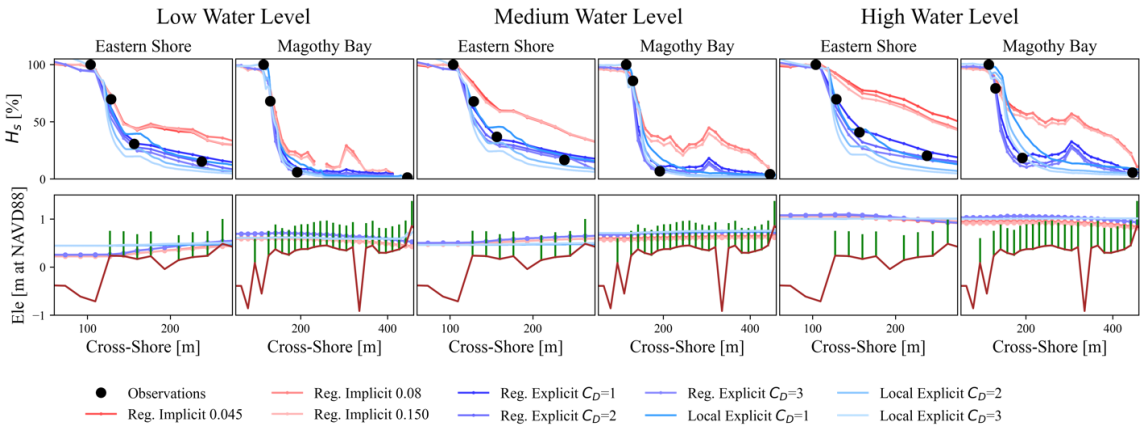

Figure 10 Water Level Conditions at Max Wave Height. (Left) Low water level at max wave heights. (Middle) Medium water level at max wave heights. (Right) High Water Level at max wave heights.

The relative bias was calculated for Eastern Shore and Magothy Bay during the high wave heights and water level conditions in Figure 11. Eastern Shore, during the low water levels had small biases to the observations for all schemes, with the regional implicit schemes being the largest at 20% for station 3 and increasing slightly to 25% at station 4. Furthermore, the medium and high-water levels follow a similar trend with regional implicit schemes showing an underestimation in the attenuation at stations 2, 3, and 4. Magothy Bay, the low water level condition the regional implicit schemes and the explicit schemes show little bias in the attenuation except at station 3 where the regional implicit schemes and the local explicit C_D=1 underestimates the attenuation close to 20%. Moreover, during the medium water level and high-water level conditions the differences between the regional implicit schemes and the explicit schemes increase after station 2.

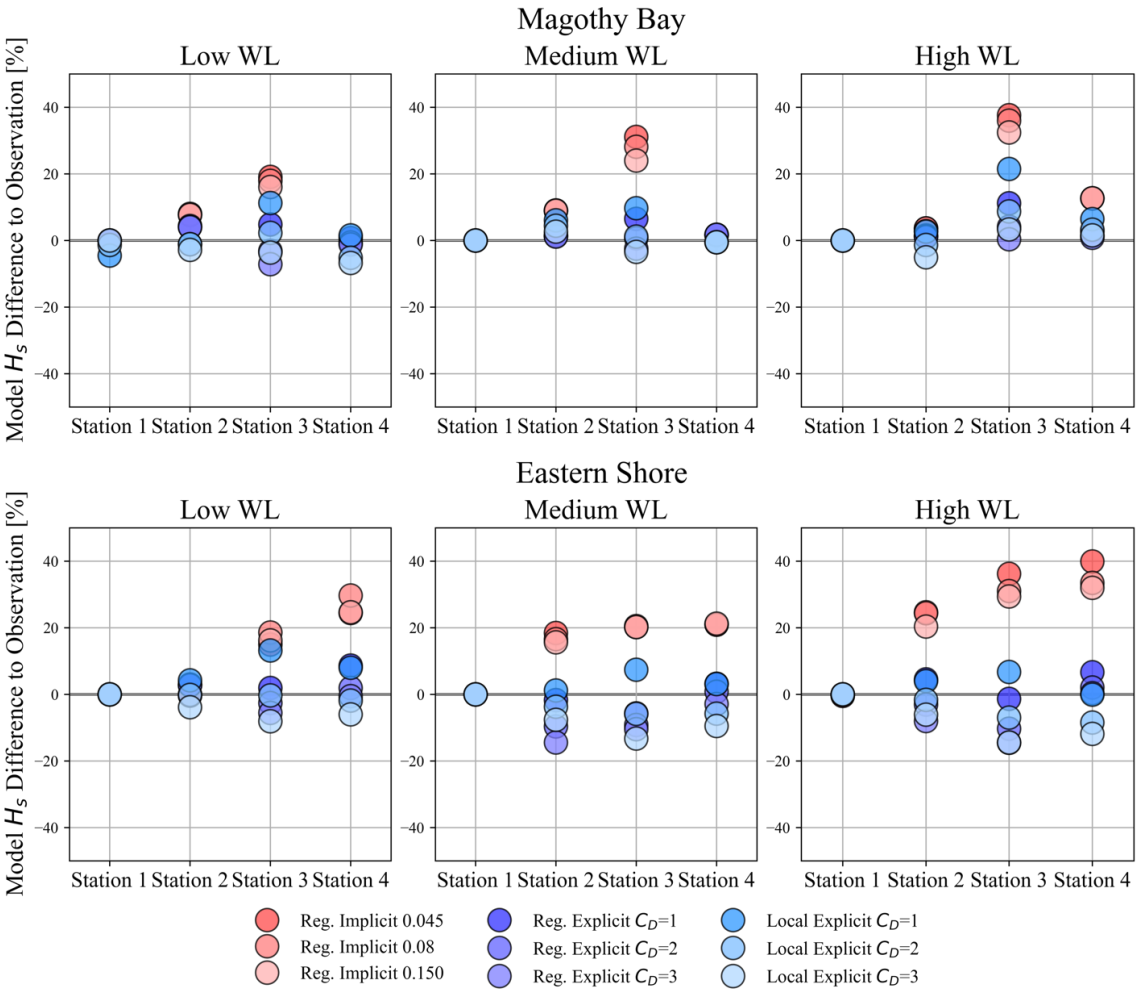

Figure 11 Water Level Condition for Max Wave Attenuation Relative Bias at Magothy Bay and Eastern Shore. (Left) Low water level at max wave heights. (Middle) Medium water level at max wave heights. (Right) High Water Level at max wave heights.

The water level conditions that were evaluated for the distance to fully attenuate the waves in the marsh for each scheme in figure 12. Eastern Shore, the high-water level condition the regional implicit schemes attenuated waves at 480m, while the regional explicit schemes attenuated the waves 150m earlier within 330m in the marsh. The local explicit schemes attenuated the waves the earliest by almost 45m to the regional explicit schemes

whereas there were further differences to the regional implicit by 185m. As the water level conditions decreased the attenuation distance also decreased, the regional implicit schemes for both the medium and low water level conditions attenuated the waves at 300m, while during the medium water level the regional explicit schemes attenuated the waves 15m before the regional implicit. The local explicit at the medium water level condition maintained attenuation earliest by 15m to the regional explicit and 30m to the regional implicit. The low water level condition the regional explicit attenuated the waves at the same distance during the medium water levels, but the local explicit attenuated the waves even earlier by 70m to the regional explicit and 90m to the regional implicit. At Magothy Bay, during the high and medium water levels the regional implicit schemes show full attenuation at 480m and could be due to the levee in this marsh. The regional explicit schemes, during the high-water level condition, show full attenuation by 40m to the regional implicit, and the local explicit attenuated the waves earlier by 105m to the regional explicit and 145m to the regional implicit. The medium water level condition the regional explicit attenuated the waves slightly earlier then the high-water level condition and by 60m to the regional implicit. The local explicit maintained the earliest attenuation during the medium water level condition by 130m to the regional explicit and 190m to the regional implicit. However, during the low water level condition at Magothy Bay the different schemes start to show different behaviors. The regional implicit now attenuates the waves 430m which is 20m sooner than the other conditions. The regional explicit attenuated the 230m earlier to the implicit, while the local explicit attenuated the waves only 10m sooner than the regional explicit.

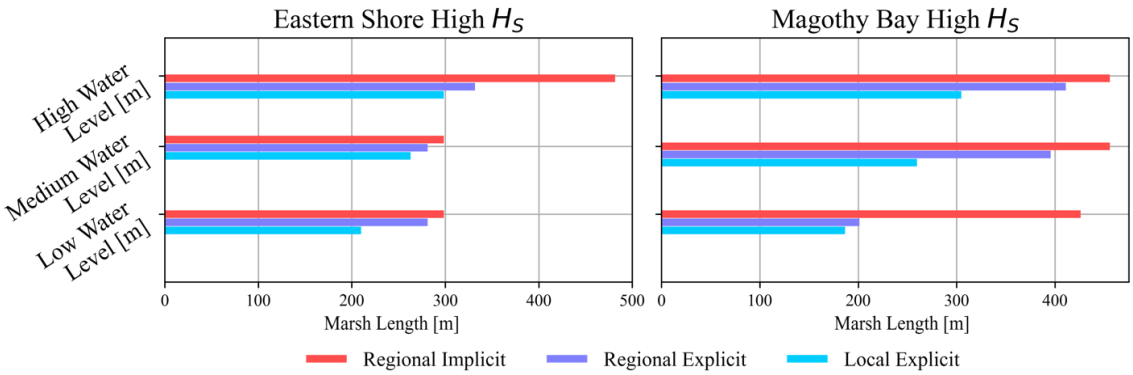

Figure 12 Wave Attenuation Lengths for different water levels at the max wave heights. (Left) Eastern Shore wave attenuation length. (Right) Magothy Bay wave attenuation length.

3.3.2 Medium Wave Height Conditions

Next, the water level conditions at the medium wave heights are shown in figure 13 as a function of the distance within the marsh. Eastern Shore, the low water condition shows further reduced differences between the regional implicit schemes and the explicit schemes then during the high wave conditions shown earlier. During the medium water level, the differences between the regional implicit schemes and the explicit schemes increases. The regional explicit schemes are showing slight underestimation in the wave heights as the waves travel throughout the marsh, whereas the local explicit C_D=2 and C_D=3 present accurate attenuation to the observations. The medium water level condition, the regional implicit schemes diverge further from the explicit schemes and also show that the higher friction has a slightly more attenuation. The explicit schemes show similar results to the low water level conditions where the regional explicit is slightly underestimating the

attenuation while the local explicit C_D=2 and C_D=3 are capturing the attenuation. The last condition for Eastern Shore, the high water level, the difference between the regional implicit schemes and the explicit schemes show the greatest difference, 7% at station 2 and close to about 25% at stations 3 and 4. The regional explicit schemes capture the observations, while the local explicit C_D=1 underestimate and C_D=3 overestimate the wave attenuation with only C_D=2 accurately capturing the attenuation at stations 3 and 4. Magothy Bay, the low water level shows a small difference between the regional implicit and the explicit schemes, except for a dynamic showing between station 3 and 4 when the regional implicit schemes show a sudden decrease in the wave attenuation. During the medium water level condition, the results show an increase difference between the regional implicit schemes and the explicit schemes starting a little before station 3 and throughout to station 4. The regional schemes accurately predict the wave attenuation at both station 3 and 4, but the local explicit C_D=1 slightly underestimates the wave attenuation at station 3. For the final condition, the high-water levels at Magothy Bay, the difference increases further between the regional implicit schemes and the explicit schemes close to 25%. The regional explicit C_D=1 and C_D=2 predict the wave attenuation to the observations while C_D=3 slightly overestimate the attenuation at station 3. The local explicit schemes C_D=2 and C_D=3 predict the attenuation whereas C_D=1 underestimate the attenuation at station 3.

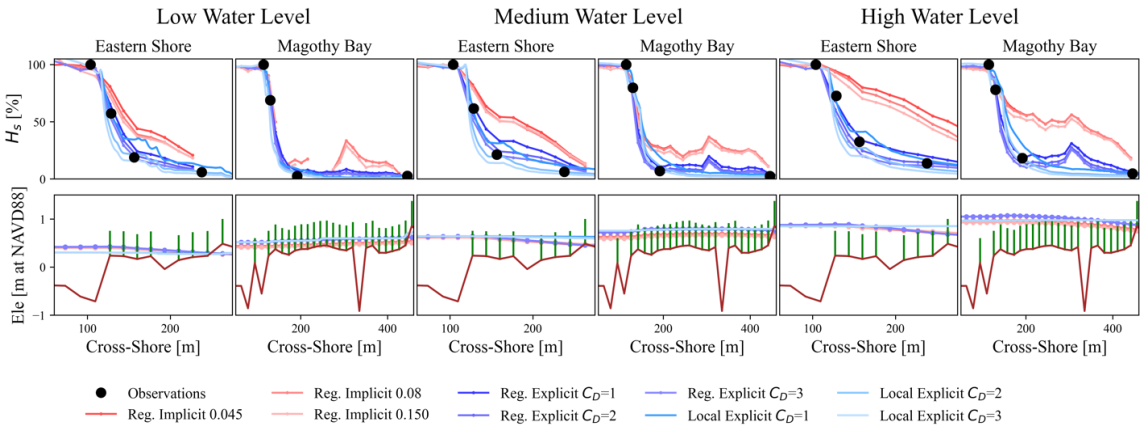

Figure 13 Water Level Conditions at Medium Wave Height. (Left) Low water level at medium wave heights. (Middle) Medium water level at medium wave heights. (Right) High Water Level at medium wave heights.

The relative bias was calculated for Eastern Shore and Magothy Bay during the medium wave heights and water level conditions in figure 14. Eastern Shore, during the low water levels had small biases to the observations for all schemes, with the regional implicit schemes being the largest at 20% for station 3 and increasing slightly to 25% at station 4. Furthermore, the medium and high water levels follow a similar trend with regional implicit schemes showing an underestimation in the attenuation at stations 2, 3, and 4. The regional explicit schemes maintained a relative bias of 10% during the low water level conditions, and during the medium water level conditions the bias increased at station 3 and 4 to 10%. The local explicit schemes during the medium water level condition showed only slight bias to the observations overestimation of the attenuation at station 2 and staying close to 5% bias for stations 3 and 4. However, during the high water level conditions the regional explicit schemes bias reduced the underestimation and showed more overestimation in the attenuation at stations 3 and 4, whereas the local explicit schemes

showed lower bias at station 2 but overestimation of the attenuation at stations 3 and 4. Magothy Bay, the low water level condition the regional implicit schemes and the explicit schemes show little bias in the attenuation except at station 3 where the regional implicit schemes underestimates the attenuation close to 15%. Moreover, during the medium water level and high-water level conditions the differences between the regional implicit schemes and the explicit schemes increase after station 2 to a 20% bias. The high water level condition the implicit showed the greatest difference to the observations with a bias of 36% at station 3 and 15% at station 4. The regional and local explicit schemes maintained to stay within a 5% bias for all the stations, except for local explicit C_D=1 underestimating at station 3.

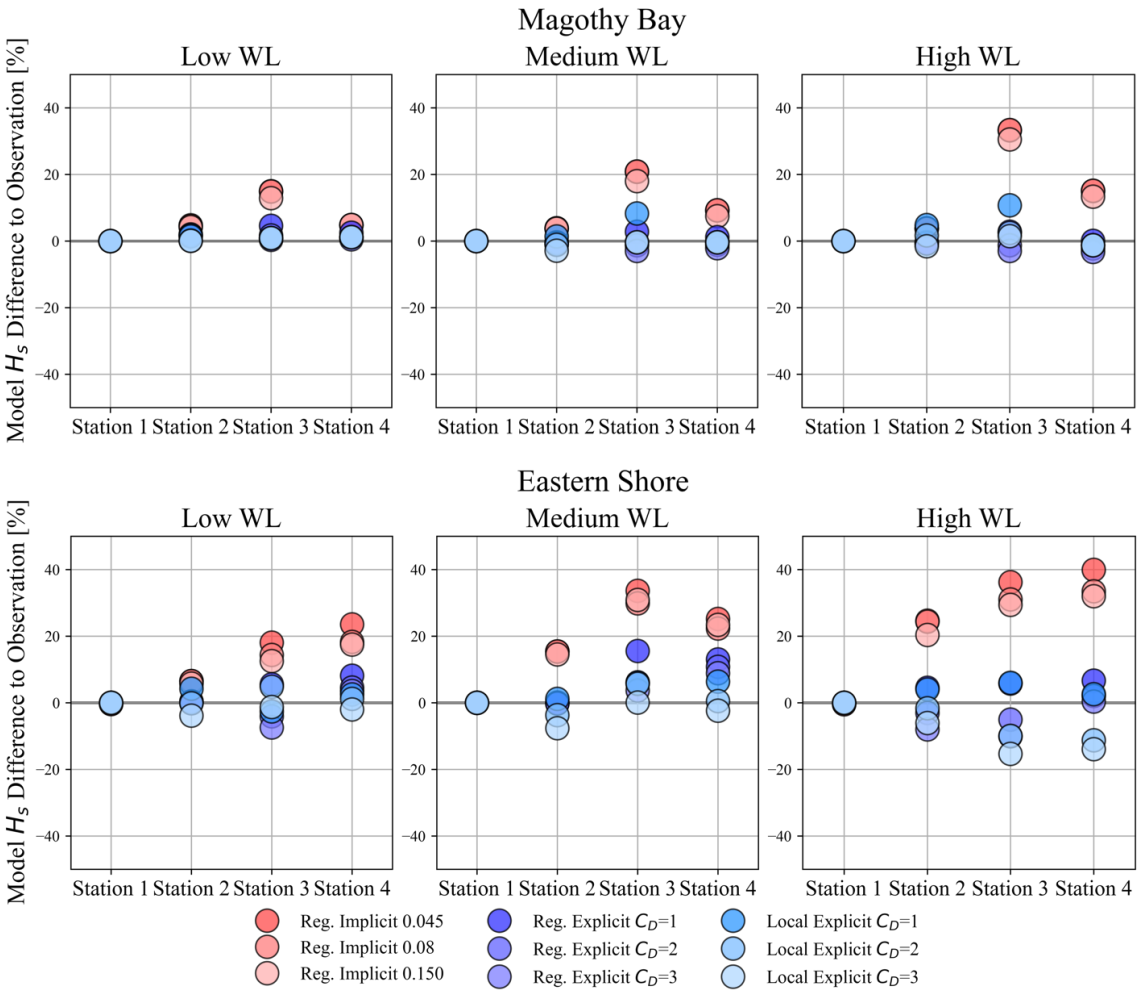

Figure 14 Water Level Condition for Medium Wave Attenuation Relative Bias at Magothy Bay and Eastern Shore. (Left) Low water level at medium wave heights. (Middle) Medium water level at medium wave heights. (Right) High Water Level at medium wave heights.

The water level conditions that were evaluated for the distance to fully attenuate the medium waves in the marsh for each scheme in figure 15. Eastern Shore, the high-water level condition the regional implicit schemes attenuated waves at 480m, while the regional explicit schemes attenuated the waves 180m earlier then regional implicit schemes at a distance within 300m in the marsh. The local explicit schemes attenuated the waves the earliest by almost 35m to the regional explicit schemes whereas the difference to the regional implicit by 225m.

Furthermore, as the water level conditions decreased the attenuation distance also decreased, the regional implicit schemes for both the medium and low water level conditions attenuated the waves at 300m, while during the medium water level the regional explicit schemes attenuated the waves 40m before the regional implicit. The local explicit at the medium water level condition attenuation earliest by 15m to the regional explicit and 55m to the regional implicit. The low water level condition the regional explicit attenuated the waves slightly earlier then the medium water level condition at a distance of 230m within the marsh 70m before the regional implicit schemes, but the local explicit attenuated the waves even earlier by 40m to the regional explicit and 110m to the regional implicit. Magothy Bay, during the high-water levels the regional implicit schemes show full attenuation at 480m and could be due to the levee in this marsh. The regional explicit schemes show full attenuation by 110m earlier than the regional implicit schemes, and the local explicit schemes attenuated the waves earlier by 90m to the regional explicit and 200m to the regional implicit. The medium water level condition the regional implicit schemes started to show attenuation earlier in the marsh, 430m. The regional explicit attenuated the waves by 140m before the regional implicit. The local explicit maintained the earliest attenuation during the medium water level condition by attenuating the waves 85m earlier than the regional explicit and 225m to the regional implicit. However, during the low water level condition at Magothy Bay the regional implicit now attenuates the waves 300m which is +120m sooner than the other conditions. The regional explicit attenuated the 100m earlier to the regional implicit, while the local explicit attenuated the waves only 25m sooner than the regional explicit and 125m to the regional implicit.

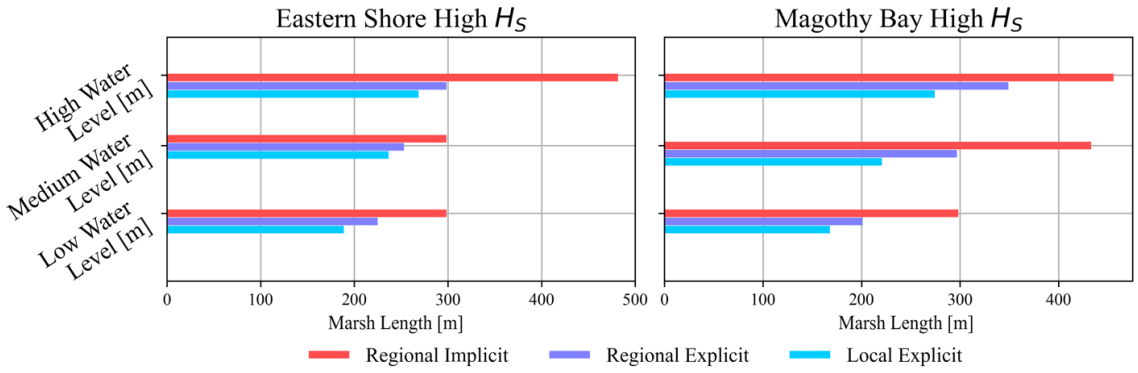

Figure 15 Wave Attenuation Lengths for different water levels at the medium wave heights. (Left) Eastern Shore wave attenuation length. (Right) Magothy Bay wave attenuation length.

3.3.3 Low Wave Height Conditions

Lastly, the water level conditions at the low wave heights are shown in figure 16 as a function of the distance within the marsh. Eastern Shore, the low water condition shows further reduced differences between the regional implicit schemes and the explicit schemes then during the medium and high wave conditions. During the medium water level, the differences between the regional implicit schemes and the explicit schemes increases. The regional explicit schemes showed underestimation in the wave attenuation at station 3 and further underestimation at station 4, whereas the local explicit C_D=2 and C_D=3 present accurate attenuation to the observations. The medium water level condition, the regional implicit schemes diverge further from the explicit schemes, while the regional explicit schemes are underestimating the attenuation at stations 3 and 4, and the local explicit C_D=3 is capturing the observed attenuation. The last condition for Eastern Shore, the high water level, the difference between the regional implicit schemes and the explicit schemes show

the greatest difference, 7% at station 2 and close to about 20% at stations 3 and 4. The regional explicit schemes capture the observations, while the local explicit C_D=1 underestimate and C_D=3 overestimate the wave attenuation with only C_D=2 accurately capturing the attenuation at stations 3 and 4. Magothy Bay, the low water level shows a small difference between the regional implicit and the explicit schemes, except for a dynamic showing between station 3 and 4 when the regional implicit schemes show a sudden decrease in the wave attenuation. During the medium water level condition, the results show an increase difference between the regional implicit schemes and the explicit schemes starting a little before station 3 and throughout to station 4. The regional schemes accurately predict the wave attenuation at both station 3 and 4, but the local explicit C_D=1 slightly underestimates the wave attenuation at station 3. For the final condition, the high-water levels at Magothy Bay, the difference increases further between the regional implicit schemes and the explicit schemes close to 20%. The regional explicit C_D=1 and C_D=2 predict the wave attenuation to the observations while C_D=3 slightly overestimate the attenuation at station 3. The local explicit schemes C_D=2 and C_D=3 predict the attenuation whereas C_D=1 underestimate the attenuation at station 3.

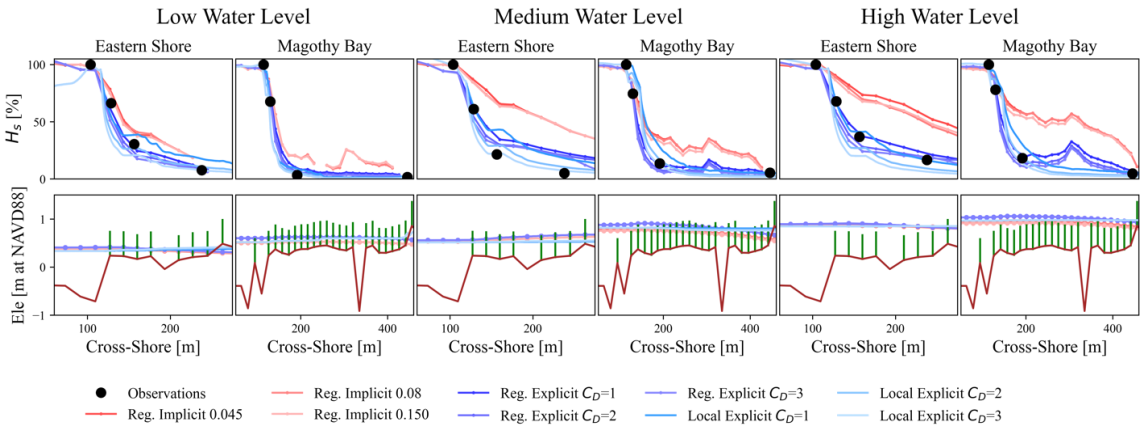

Figure 16 Water Level Conditions at Low Wave Height. (Left) Low water level at low wave heights. (Middle) Medium water level at low wave heights. (Right) High Water Level at low wave heights.

The relative bias was calculated for Eastern Shore and Magothy Bay during the low wave heights and varying water level conditions in Figure 17. Eastern Shore, during the low water levels had small biases to the observations for all schemes, with the regional implicit schemes being the largest at 17% for station 3 and decreasing slightly to 15% at station 4. Furthermore, the medium and high-water levels follow a similar trend with regional implicit schemes showing an underestimation in the attenuation at stations 2, 3, and 4. The regional explicit schemes maintained a relative bias of 10% during the low water level conditions, and during the medium water level conditions the bias increased at stations 3 and 4 to 18%. The local explicit schemes during the medium water level condition showed only slight bias to the observations of the attenuation at station 2 and staying close to 5% bias for stations 3 and 4. However, during the high water level conditions the regional explicit schemes bias reduced the underestimation and showed more overestimation in the attenuation at stations 3 and 4, whereas the local explicit schemes showed lower bias at station 2 but overestimation of the attenuation at stations 3 and 4. Magothy Bay, the low

water level condition the regional implicit schemes and the explicit schemes show little bias in the attenuation except at station 3 where the regional implicit schemes underestimates the attenuation close to 15%. Moreover, during the medium and high-water level conditions the differences between the regional implicit schemes and the observations increase after station 2 to 20% bias. The high-water level condition the implicit showed the greatest difference to the observations with a bias of 34% at station 3 and 10% at station 4. The regional and local explicit schemes maintained to stay within a 5% bias for all the stations, except for local explicit C_D=1 underestimating at station 3.

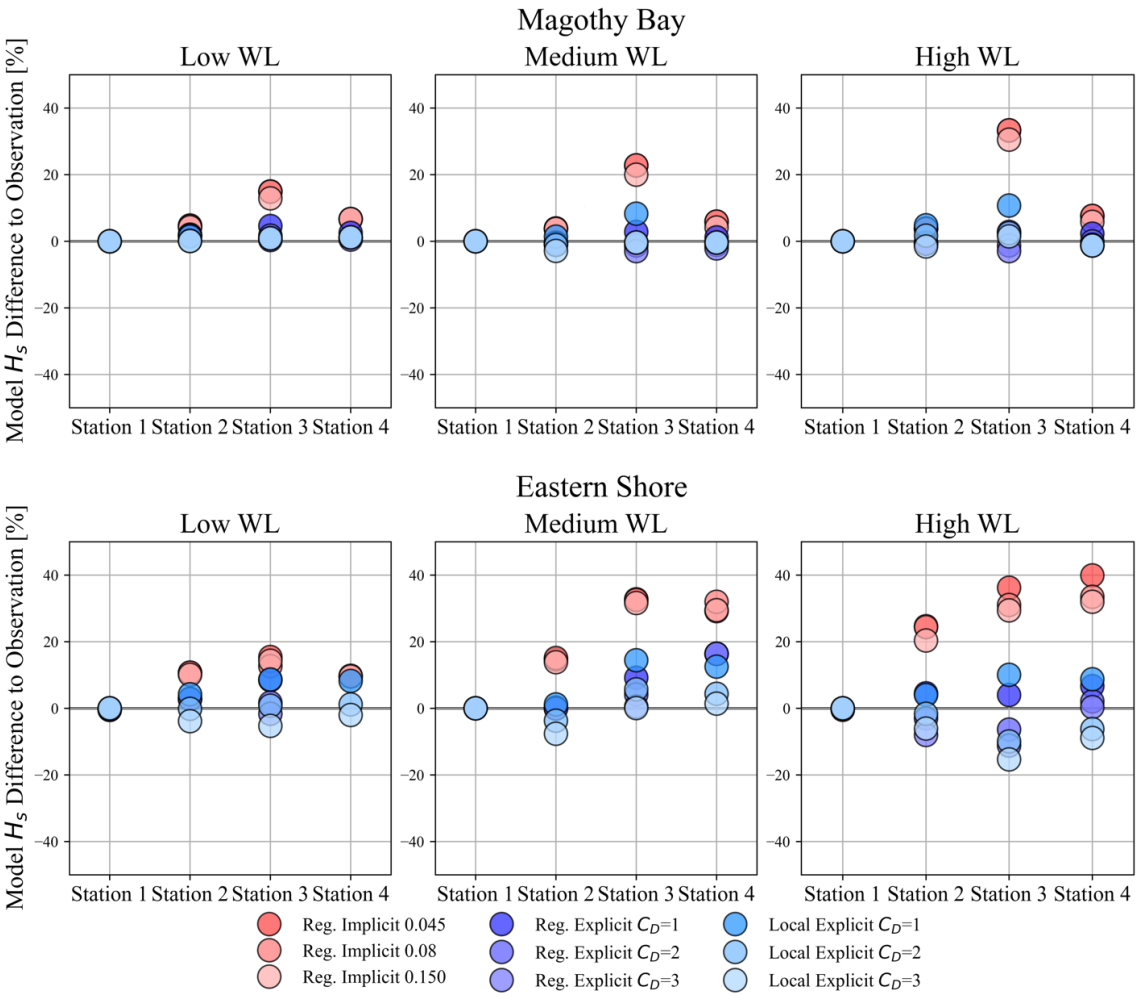

Figure 17 Water Level Condition for Low Wave Attenuation Relative Bias at Magothy Bay and Eastern Shore. (Left) Low water level at low wave heights. (Middle) Medium water level at low wave heights. (Right) High Water Level at low wave heights.

The water level conditions that were evaluated for the distance to fully attenuate the waves in the marsh for each scheme during low wave heights shown in figure 18. Eastern Shore, the high-water level condition the regional implicit schemes attenuated waves at 380m, while the regional explicit schemes attenuated the waves 85m earlier in the marsh. The local explicit schemes attenuated the waves the earliest by almost 90m to the regional

explicit schemes whereas there were further differences to the regional implicit by 175m. As the water level conditions decreased the attenuation distance also decreased, the regional implicit schemes for the medium water level conditions attenuated the waves at 300m, while regional explicit schemes attenuated the waves 40m before the regional implicit. The local explicit at the medium water level maintained attenuation earliest by 100m to the regional explicit and 140m to the regional implicit. The low water level condition the regional implicit attenuated the waves at 240m in the marsh. The regional explicit attenuated the wave 60m earlier than the regional implicit, whereas the local explicit attenuated the waves 30m sooner than the regional explicit and 90m to the regional implicit. Magothy Bay, during the high water levels the regional implicit schemes show full attenuation at 480m and could be due to the levee in this marsh. The regional explicit schemes, during the high water level condition, show full attenuation 130m to the regional implicit, and the local explicit attenuated the waves earlier by 100m to the regional explicit and 230m to the regional implicit. The medium water level condition the regional implicit showed attenuation the earliest out of all the wave conditions at 320m. The regional explicit attenuated the waves dramatically earlier then the high-water level condition and by 150m to the regional implicit. The local explicit maintained the earliest attenuation during the medium water level condition by 40m to the regional explicit and 190m to the regional implicit. However, during the low water level condition at Magothy Bay the different schemes start to show different behaviors. The regional implicit now attenuates the waves at 240m. The regional explicit attenuated the 100m earlier to the implicit, while the local explicit attenuated the waves at the same distance of the regional explicit schemes.

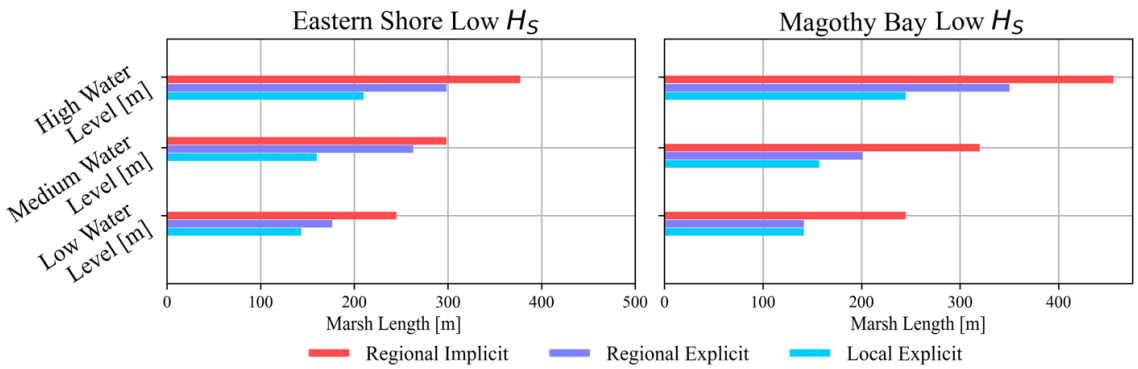

Figure 18 Wave Attenuation Lengths for different water levels at the low wave heights. (Left) Eastern Shore wave attenuation length. (Right) Magothy Bay wave attenuation length.

3.4 Implications of Implicit and Explicit schemes on Wave Attenuation

Through the evaluation of the varying water level and wave height conditions, the average expected attenuation length for the regional and local model schemes can be determined. The wave attenuation length for the regional model schemes and the local model explicit scheme shows the expected length it would take to attenuate for the three different water levels in figure 19. During the high-water level conditions at Eastern Shore the regional implicit is expected to attenuate all the waves by 450m, the regional explicit is expected to attenuate all waves between 250m to 290m, and the local explicit is expected to attenuate waves between 200m to 240m. Eastern Shore the Regional implicit decreases in difference as the water level decreases compared to both the regional and local explicit schemes. The Regional explicit maintains around a 60m difference to the local explicit for all water levels. Magothy Bay, during the high water level condition, the regional implicit follows

the same pattern as the Eastern Shore site where the difference to the local explicit decreases as the water level decreases. The regional explicit maintains a 65m difference to the local explicit for the medium and high water levels, but during the low water level there is only a 5m difference.

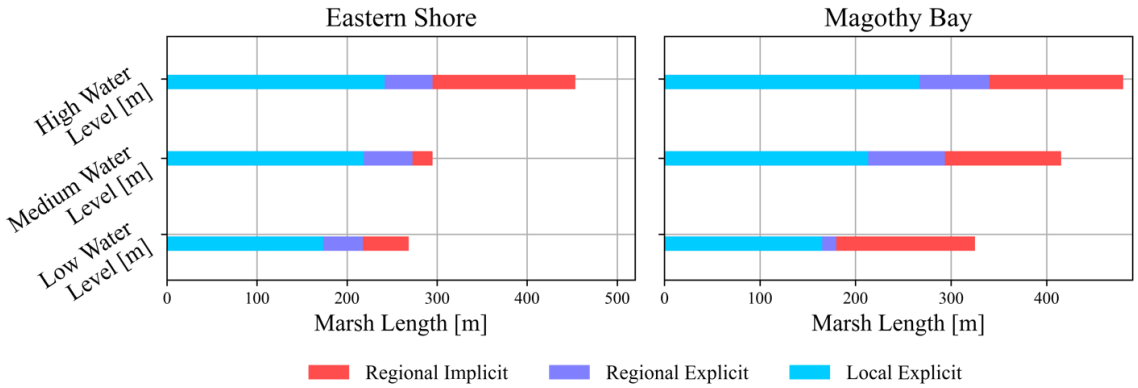

Figure 19 Average Wave Attenuation length for all conditions. (Left) Eastern Shore wave attenuation length. (Right) Magothy Bay wave attenuation length.

CHAPTER FOUR: DISCUSSION

The results of this study show that regional numerical models can accurately simulate wave attenuation by vegetation when applying the explicit schemes and that the implicit scheme can be used to identify the potential protection a marsh can provide. Through the regional model domain applying the implicit schemes, the wave attenuation by the bottom friction showed an average 30% difference to the all the wave heights during the high water levels conditions and the differences reduced as the water level and wave height decreased.

Figures 6 and 7 display that the models and the schemes used differed in the magnitude of wave dissipation throughout the marsh. While the explicit representation showed that a majority of the interaction between the waves and vegetation happened in the first 100m of the marsh (figure 7), the implicit representation is initially impacted by the dissipation at the edge of the marsh and after retains a constant attenuation coefficient throughout the marsh. The vegetation does become the dominant form of dissipation after the edge of the marsh, but the amount of dissipation that the vegetation is responsible for, in the implicit representation, is a significant difference from that in the explicit representation. Baron-hyppolite et al., 2018 reported that the implicit schemes almost represent the marsh as an intertidal mudflat since there is no significant attenuation of the wave heights. However, this study did not calculate if, through the implicit approach, the marsh would attenuate the waves. The results from this study indicate that the implicit schemes do not accurately represent the wave attenuation curve provided be the explicit schemes but are able to show

that the marshes with lengths over 400m are able to attenuate the waves (figure 19) and can be used to determine the potential benefits they have on communities.

Depth-induced breaking in the models was zero for all conditions and was not a significant source of dissipation during the medium and high-water level conditions in this system. The lower water level encountered some wave breaking at the start of the marsh sites dissipating some of the wave energy before being dissipated by the vegetation schemes. The explicit schemes were able to closely represent the observed wave heights, during different water levels, the bulk drag coefficient is held constant, would overestimate or slightly underestimate the attenuation in the marsh. This is due to the bulk drag coefficient being constant in the numerical model, but in the field sites, the bulk drag coefficient is influenced by the ratio of the water depth and the plant height (Garzon et al. 2019). In this study, the local XBeach model applying the explicit approach used a constant bulk drag coefficient, but in Garzon et al. 2018 XBeach was modified to calculate the bulk drag coefficient with different bulk drag coefficient expressions for *Spartina Alterniflora* dominated environments considering the varying water depths that are found in the field sites, this would allow for more accurate calculations of the wave attenuation.

The study sites exhibit different marsh characteristics that can influence the wave attenuation observed, such as topography, fetch length and direction, and vegetation (Glass et al., 2018). The Eastern Shore study site had characteristics such as a 0.9-m cliff marsh edge and a relatively flat marsh platform with an average slope of 0.014% (between station 2, S2, and station 4, S4). Magothy Bay, this marsh site is characterized by a steep edge formed by an ascendant slope at the seaside and a descendant slope at the land side. A flat

marsh platform is present at the landside of the marsh and several channels within the marsh platform are observed flooding in the marsh during higher water levels. The backside of the marsh is limited by a levee. These different characteristics at the marsh sites could cause complete attenuation due to topography that have been studied by Möller & Spencer, 2002 where on such marsh feature is the edge. This marsh edge not only will dissipate the waves but will also reflect the waves affecting the incoming wave heights. To avoid most of the wave attenuation at the edge of the marsh by evaluating the different water level and wave conditions. With the assumption that in figure 7 the steep slopes of the attenuation coefficient at Eastern Shore and Magothy Bay are due to the edge of the marsh, and after that the coefficient is only due to vegetation or friction. The attenuation coefficients imply that Eastern Shore has more potential for using the implicit schemes then Magothy Bay since there is a coefficients difference of 0.05 to the observation, while there is a difference of 0.25 at Magothy Bay to the observations.

CHAPTER FIVE: CONCLUSION

In this study, the accuracy of different schemes to represent wave attenuation by vegetation and varying geographical modeling domains were analyzed. The wave attenuation was modeled in one of two ways: (1) implicit, wave attenuation using a coefficient of friction; or (2) explicit, wave attenuation using "site-specific" vegetation characteristics measured at the field sites such as stem diameter, stem height, and plant density. The varying modeling domains encompassed regional scale that is bounded for the United States East Coast, and a site-specific domain or local scale.

Ultimately, the expected results from this study found that the explicit approach and finer resolution models improved the accuracy of the modeled wave attenuation. However, when looking at geographically larger perspectives, the implicit approach would provide a 30% underestimation of the wave attenuation but for marshes larger than 400m, it will show full attenuation, which would still provide guidance on possible protection strategies for communities. The explicit schemes provide the most accurate representation of the wave attenuation found in marshes, but the lack of scaled-up vegetation data hinders regionally explicitly representing the vegetation, which would provide the most accurate guidance on the potential benefits marshes can provide communities.

REFERENCES

Anderson, M. E., & Smith, J. M. (2014). Wave attenuation by flexible, idealized salt marsh vegetation. *Coastal Engineering*, *83*, 82–92. https://doi.org/10.1016/j.coastaleng.2013.10.004

Andrews, D. G., & Mcintyre, M. E. (1978). An exact theory of nonlinear waves on a Lagrangian-mean flow. *Journal of Fluid Mechanics*, *89*(4), 609–646. https://doi.org/10.1017/S0022112078002773

Arkema, K. K., Guannel, G., Verutes, G., Wood, S. A., Guerry, A., Ruckelshaus, M., Kareiva, P., Lacayo, M., & Silver, J. M. (2013). Coastal habitats shield people and property from sea-level rise and storms. *Nature Climate Change*, *3*(10), 913–918. https://doi.org/10.1038/nclimate1944

Baron-hyppolite, C., Lashley, C. H., Garzon, J., Miesse, T., Ferreira, C., & Bricker, J. D. (2018). *Comparison of Implicit and Explicit Vegetation Representations in SWAN Hindcasting Wave Dissipation by Coastal Wetlands in Chesapeake Bay*. https://doi.org/10.3390/geosciences9010008

Berg, R. J. (2016). Hurricane Joaquin (AL112015). *National Hurricane Center Tropical Cyclone Report*, *January*, 36.

Blake, E. S. (2015). *National Hurricane Center Tropical Cyclone Report. Hurricane Lowell*. *October*, 1–32. https://www.nhc.noaa.gov/data/tcr/AL122017_Jose.pdf

Blanton, B., Stillwell, L., Roberts, H., Atkinson, J., Zou, S., Forte, M., Hanson, J., & Luettich, R. (2011). *Coastal Storm Surge Analysis : Computational System Coastal and Hydraulics Laboratory Coastal Storm Surge Analysis : Computational System*. *1*.

Booij, N., Ris, R. C., & Holthuijsen, L. H. (1999). A third-generation wave model for coastal regions. *Journal of Geophical Research*, *104*(C4), 7649–7666. https://doi.org/0148-0227/99/98JC-02622

Bouma, T. J., De Vries, M. B., & Herman, P. M. J. (2010). Comparing ecosystem engineering efficiency of two plant species with contrasting growth strategies. *Ecology*, *91*(9), 2696–2704. https://doi.org/10.1890/09-0690.1

Cavaleri, L., Abdalla, S., Benetazzo, A., Bertotti, L., Bidlot, J. R., Breivik, Carniel, S., Jensen, R. E., Portilla-Yandun, J., Rogers, W. E., Roland, A., Sanchez-Arcilla, A., Smith, J. M., Staneva, J., Toledo, Y., van Vledder, G. P., & van der Westhuysen, A. J. (2018). Wave modelling in coastal and inner seas. *Progress in Oceanography*, *167*(September 2017), 164–233. https://doi.org/10.1016/j.pocean.2018.03.010

Chesapeake Bay Program. (2018). *Quick Reference Guide for Best Management Practices*.

Crooks, S., Sutton-Grier, A. E., Troxler, T. G., Herold, N., Bernal, B., Schile-Beers, L., & Wirth, T. (2018). Coastal wetland management as a contribution to the US National Greenhouse Gas Inventory. *Nature Climate Change*, *8*(12), 1109–1112. https://doi.org/10.1038/s41558-018-0345-0

Daly, C., Roelvink, D., van Dongeren, A., van Thiel de Vries, J., & McCall, R. (2012).

Validation of an advective-deterministic approach to short wave breaking in a surf-beat model. *Coastal Engineering*, *60*(1), 69–83. https://doi.org/10.1016/j.coastaleng.2011.08.001

Danielson, J. J., Poppenga, S. K., Brock, J. C., Evans, G. A., Tyler, D. J., Gesch, D. B., Thatcher, C. A., & Barras, J. A. (2016). Topobathymetric elevation model development using a new methodology: Coastal national elevation database. *Journal of Coastal Research*, *76*(sp1), 75–89. https://doi.org/10.2112/SI76-008

De Oude, R. (2010). *Modelling wave attenuation by vegetation with SWAN-VEG: Model evaluation and application to the Noordwaard polder*. *January*, 116.

DING, Y., OWENSBY, M. B., ZHU, L., CHEN, Q., & JOHNSON, B. D. (2019). MODELING WAVE ATTENUATION AND RUNUP DUE TO WAVE-CURRENT-VEGETATION INTERACTION. *Coastal Sediments 2019, 2011*, 1528–1537. https://doi.org/10.1142/9789811204487_0132

Ding, Y., Rosati, J. D., Zhu, L., & Chen, Q. (2019). Modeling Wave Attenuation and Runup in Wetland and Vegetated Coast. *World Environmental and Water Resources Congress 2019*, 426–436. https://doi.org/10.1061/9780784482353.040

Feagin, R. A., Lozada-Bernard, S. M., Ravens, T. M., Moller, I., Yeager, K. M., & Baird, A. H. (2009). Does vegetation prevent wave erosion of salt marsh edges? *Proceedings of the National Academy of Sciences*, *106*(25), 10109–10113. https://doi.org/10.1073/pnas.0901297106

Ferreira, C. M., Irish, J. L., & Olivera, F. (2014). Uncertainty in hurricane surge simulation due to land cover specification. *Journal of Geophysical Research: Oceans*, *119*(3), 1812–1827. https://doi.org/10.1002/2013JC009604

Garzon, J. L., Ferreira, C. M., Maza, M. E., Lara, J. L., & Losada, I. (2019). Wave attenuation by Spartina saltmarshes in the Chesapeake Bay under storm surge conditions (Under review). *Journal of Geophysical Research: Oceans*, *124*. https://doi.org/10.1029/2018JC014865

Garzon, J.L., Maza, M., Ferreira, C. M., Lara, J. L., & Losada, I. J. (2019). Wave attenuation by Spartina saltmarshes in the Chesapeake Bay under storm surge conditions. *Journal of Geophysical Research: Oceans*, 1–24. https://doi.org/10.1029/2018jc014865

Garzon, Juan L., Ferreira, C. M., & Padilla-Hernandez, R. (2018). Evaluation of weather forecast systems for storm surge modeling in the Chesapeake Bay. *Ocean Dynamics*, *68*(1), 91–107. https://doi.org/10.1007/s10236-017-1120-x

Garzon, Juan L., Miesse, T., & Ferreira, C. M. (2018). Field-based numerical model investigation of wave propagation across marshes in the Chesapeake Bay under storm conditions. *Coastal Engineering*, *146*(November 2018), 32–46. https://doi.org/10.1016/j.coastaleng.2018.11.001

Glass, E. M., Garzon, J. L., Lawler, S., Paquier, E., & Ferreira, C. M. (2018). Potential of marshes to attenuate storm surge water level in the Chesapeake Bay. *Limnology and Oceanography*, *63*(2), 951–967. https://doi.org/10.1002/lno.10682

Gorrell, L., Raubenheimer, B., Elgar, S., & Guza, R. T. (2011). SWAN predictions of waves observed in shallow water onshore of complex bathymetry. *Coastal Engineering*, *58*(6), 510–516. https://doi.org/10.1016/j.coastaleng.2011.01.013

Hladik, C., Schalles, J., & Alber, M. (2013). Salt marsh elevation and habitat mapping using hyperspectral and LIDAR data. *Remote Sensing of Environment*, *139*, 318–330. https://doi.org/10.1016/j.rse.2013.08.003

Holthuijsen, L. H., Booij, N., & Herbers, T. H. C. (1989). A prediction model for stationary, short-crested waves in shallow water with ambient currents. *Coastal Engineering*, *13*(1), 23–54. https://doi.org/10.1016/0378-3839(89)90031-8

Jacobsen, N. G., Bakker, W., Uijttewaal, W. S. J., & Uittenbogaard, R. (2019). Experimental investigation of the wave-induced motion of and force distribution along a flexible stem. *Journal of Fluid Mechanics*, 1036–1069. https://doi.org/10.1017/jfm.2019.739

Jadhav, R., & Chen, Q. (2012). Field Investigation of Wave Dissipation Over Salt Marsh Vegetation During Tropical Cyclone. *Coastal Engineering Proceedings*, 1–11. http://journals.tdl.org/icce/index.php/icce/article/view/6575

Jin, S., Homer, C., Yang, L., Danielson, P., Dewitz, J., Li, C., Zhu, Z., Xian, G., & Howard, D. (2019). Overall methodology design for the United States national land cover database 2016 products. *Remote Sensing*, *11*(24). https://doi.org/10.3390/rs11242971

Jonsson, I. G., & Carlsen, N. A. (1976). EXPERIMENTAL AND THEORETICAL INVESTIGATIONS IN AN OSCILLATORY TURBULENT BOUNDARY LAYER. *Journal of Hydraulic Research*, *14*(1), 45–60. https://doi.org/10.1080/00221687609499687

Kamphuis, J. W. (2010). Introduction to Coastal Engineering and Management. In *Advanced Series on Ocean Engineering: Vol. Volume 30*. WORLD SCIENTIFIC. https://doi.org/doi:10.1142/7021

Lowe, R. J., Falter, J. L., Koseff, J. R., Monismith, S. G., & Atkinson, M. J. (2007). Spectral wave flow attenuation within submerged canopies: Implications for wave energy dissipation. *Journal of Geophysical Research: Oceans*, *112*(5), 1–14. https://doi.org/10.1029/2006JC003605

Lynn Jenner. (2019, September 9). *Dorian 2019 – Hurricane And Typhoon Updates*. NASA. https://blogs.nasa.gov/hurricanes/tag/dorian-2019/

Marsooli, R., Orton, P. M., Georgas, N., & Blumberg, A. F. (2016). Three-dimensional hydrodynamic modeling of coastal flood mitigation by wetlands. *Coastal Engineering*, *111*, 83–94. https://doi.org/10.1016/j.coastaleng.2016.01.012

Marsooli, R., Orton, P. M., Mellor, G., Georgas, N., & Blumberg, A. F. (2017). A coupled circulation-wave model for numerical simulation of storm tides and waves. *Journal of Atmospheric and Oceanic Technology*, *34*(7), 1449–1467. https://doi.org/10.1175/JTECH-D-17-0005.1

Möller, I., & Spencer, T. (2002). Wave dissipation over macro-tidal saltmarshes: Effects of marsh edge typology and vegetation change. *Journal of Coastal Research*, *36*(36), 506–521. https://doi.org/10.2112/1551-5036-36.sp1.506

Möller, Iris, Kudella, M., Rupprecht, F., Spencer, T., Paul, M., Van Wesenbeeck, B. K., Wolters, G., Jensen, K., Bouma, T. J., Miranda-Lange, M., & Schimmels, S. (2014). Wave attenuation over coastal salt marshes under storm surge conditions. *Nature Geoscience*, *7*(10), 727–731. https://doi.org/10.1038/ngeo2251

Nicole Elko, Casey Dietrich, Mary Cialone, Hilary Stockdon, & Matt W. Bilskie, Brandon Boyd, Bianca Charbonneau, Dan Cox, Kendra Dresback, Steve Elgar, Amanda Lewis, Patrick Limber, Joe Long, Chris Massey, Talea Mayo, Kathryn McIntosh, Norberto Nadal-Caraballo, Britt Raubenheimer, Tori Tomiczek, and A. W. (2019). Advancing the understanding of storm processes and impacts. *Shore & Beach*, *87*(1), 37–50.

Nowacki, D. J., Beudin, A., & Ganju, N. K. (2017). Spectral wave dissipation by submerged aquatic vegetation in a back-barrier estuary. *Limnology and Oceanography*, *62*(2), 736–753. https://doi.org/10.1002/lno.10456

Ozeren, Y., Wren, D. G., & Wu, W. (2014). Experimental Investigation of Wave Attenuation through Model and Live Vegetation. *Journal of Waterway, Port, Coastal, and Ocean Engineering*, *140*(5), 04014019. https://doi.org/10.1061/(ASCE)WW.1943-5460.0000251

Paquier, A. E., Haddad, J., Lawler, S., & Ferreira, C. M. (2017). Quantification of the Attenuation of Storm Surge Components by a Coastal Wetland of the US Mid Atlantic. *Estuaries and Coasts*, *40*(4), 930–946. https://doi.org/10.1007/s12237-016-0190-1

Roberts, K. J., Pringle, W. J., & Westerink, J. J. (2019). OceanMesh2D 1.0: MATLAB-based software for two-dimensional unstructured mesh generation in coastal ocean modeling. *Geoscientific Model Development*, *12*(5), 1847–1868. https://doi.org/10.5194/gmd-12-1847-2019

Roelvink, D., Reniers, A., van Dongeren, A., van Thiel de Vries, J., McCall, R., & Lescinski, J. (2009). Modelling storm impacts on beaches, dunes and barrier islands. *Coastal Engineering*, *56*(11–12), 1133–1152. https://doi.org/10.1016/j.coastaleng.2009.08.006

Rooijen, A., Lowe, R., Rijnsdorp, D. P., Ghisalberti, M., Jacobsen, N. G., & McCall, R. (2020). Wave-Driven Mean Flow Dynamics in Submerged Canopies. *Journal of Geophysical Research: Oceans*, *125*(3), 1–21. https://doi.org/10.1029/2019jc015935

Saha, S., Moorthi, S., Wu, X., Wang, J., Nadiga, S., Tripp, P., Behringer, D., Hou, Y. T., Chuang, H. Y., Iredell, M., Ek, M., Meng, J., Yang, R., Mendez, M. P., Van Den Dool, H., Zhang, Q., Wang, W., Chen, M., & Becker, E. (2014). The NCEP climate forecast system version 2. *Journal of Climate*, *27*(6), 2185–2208. https://doi.org/10.1175/JCLI-D-12-00823.1

Smith, J. M., Bryant, M. A., & Wamsley, T. V. (2016). Wetland buffers: Numerical modeling of wave dissipation by vegetation. *Earth Surface Processes and Landforms*, *41*(6), 847–854. https://doi.org/10.1002/esp.3904

Tarek, M., Brissette, F. P., & Arsenault, R. (2019). Evaluation of the ERA5 reanalysis as a potential reference dataset for hydrological modeling over North-America. *Hydrology and Earth System Sciences Discussions*, *July*, 1–35. https://doi.org/10.5194/hess-2019-316

Towns, J., Cockerill, T., Dahan, M., Foster, I., Gaither, K., Grimshaw, A., Hazlewood, V., Lathrop, S., Lifka, D., Peterson, G. D., Roskies, R., Scott, J. R., & Wilkens-Diehr, N. (2014). XSEDE: Accelerating scientific discovery. *Computing in Science and Engineering*, *16*(5), 62–74. https://doi.org/10.1109/MCSE.2014.80

USDA, N. (2021). *The PLANTS Database (http://plants.usda.gov)* (p. National Plant Data Team).

Van Coppenolle, R., Schwarz, C., & Temmerman, S. (2018). Contribution of Mangroves and Salt Marshes to Nature-Based Mitigation of Coastal Flood Risks in Major Deltas of the World. *Estuaries and Coasts*, *41*(6), 1699–1711. https://doi.org/10.1007/s12237-018-0394-7

van Rooijen, A. A., McCall, R. T., van Thiel de Vries, J. S. M., van Dongeren, A. R., Reniers, A. J. H. M., & Roelvink, J. A. (2016). Modeling the effect of wave-vegetation interaction on wave setup. *Journal of Geophysical Research: Oceans*, *121*(6), 4341–4359. https://doi.org/10.1002/2015JC011392

van Rooijen, A. A., van Thiel de Vries, J. S. M., McCall, R. T., van Dongeren, A. R., Roelvink, J. A., & Reniers, A. J. H. M. (2015). Modeling of wave attenuation by vegetation with XBeach. *E-Proceedings of the 36th IAHR World Congress*, 7.

Vitart, F., Balsamo, G., Bidlot, J.-R., Lang, S., Tsonevsky, I., Richardson, D., & Alonso-Balmaseda, M. (2019). Use of ERA5 to Initialize Ensemble Re-forecasts. *ECMWF Technical Memoranda*, *February*. https://www.ecmwf.int/node/18872

Vuik, V., Jonkman, S. N., Borsje, B. W., & Suzuki, T. (2016). Nature-based flood protection: The efficiency of vegetated foreshores for reducing wave loads on coastal dikes. *Coastal Engineering*, *116*, 42–56. https://doi.org/10.1016/j.coastaleng.2016.06.001

Weatherall, P., Marks, K. M., Jakobsson, M., Schmitt, T., Tani, S., Arndt, J. E., Rovere, M., Chayes, D., Ferrini, V., & Wigley, R. (2015). A new digital bathymetric model of the world's oceans. *Earth and Space Science*, *2*(8), 331–345. https://doi.org/10.1002/2015EA000107

Westerink, J. J., Luettich, R. A., Feyen, J. C., Atkinson, J. H., Dawson, C., Roberts, H. J., Powell, M. D., Dunion, J. P., Kubatko, E. J., & Pourtaheri, H. (2008). A Basin- to Channel-Scale Unstructured Grid Hurricane Storm Surge Model Applied to Southern Louisiana. *Monthly Weather Review*. https://doi.org/10.1175/2007MWR1946.1

White, S. (2007). Utilization of LIDAR and NOAA ' s Vertical Datum Delineation. *Analysis*.

Wilen, B. O., & Bates, M. K. (1995). *The US Fish and Wildlife Service's National Wetlands Inventory Project BT - Classification and Inventory of the World's Wetlands* (C. M. Finlayson & A. G. van der Valk (eds.); pp. 153–169). Springer Netherlands. https://doi.org/10.1007/978-94-011-0427-2_13

Wu, W., Ozeren, Y., Wren, D., Chen, Q., Zhang, G., Holland, M., Ding, Y., Kuiry, S. N., Zhang, M., Jadhav, R., Chatagnier, J., Chen, Y., & Gordji, L. (2011). *Investigation of Surge and Wave Reduction by Vegetation*. *80037*, 346.

Yang, S. L., Shi, B. W., Bouma, T. J., Ysebaert, T., & Luo, X. X. (2012). Wave Attenuation at a Salt Marsh Margin: A Case Study of an Exposed Coast on the Yangtze Estuary. *Estuaries and Coasts*, *35*(1), 169–182. https://doi.org/10.1007/s12237-011-9424-4

Zhang, X., & Lin, P. (2020). *Wave Attenuation by Spartina alterniflora under Macro-Tidal and Storm Surge Conditions*. 2151–2162.

BIOGRAPHY

Tyler Miesse graduated from Landstown High School, Virginia Beach, Virginia, in 2013. He received his Bachelor of Science from George Mason University in 2018. He was employed as a coastal engineer at Dewberry for a year and then received his Master of Science in Civil Engineering from George Mason University in 2021.